Influence of the initial CH4-hydrate system properties on CO2 capture kinetics

Quang-Du Le, Carla Rodriguez, Ludovic Legoix, Claire Pirim, Bertrand Chazallon

Version of Record: https://www.sciencedirect.com/science/article/pii/S0306261920313209
Manuscript_47ef2473b5887d21fa980fc51f30958d

Influence of the initial CH_4-hydrate system properties on CO_2 capture kinetics

Quang-Du Le [1], Carla T. Rodriguez [1], Ludovic Nicolas Legoix [1], Claire Pirim [1] and Bertrand Chazallon [1,*]

1 Université de Lille, CNRS, UMR 8523 – PhLAM – Laboratoire de Physique des Lasers, Atomes et Molécules, CERLA – Centre d'Etudes et de Recherche Lasers et Applications, F-59000, Lille, France;

* Correspondence to bertrand.chazallon@univ-lille.fr; Tel.: +33 (0) 3 20 33 64 68 (B.C.)

Abstract: Recovering methane from natural gas hydrate deposits using carbon dioxide injection is currently of great environmental and energetic interest as it shows potential for producing an energy resource while mitigating CO_2 emissions through CO_2 sequestration. This work investigates the exchange kinetic between CH_4 and CO_2 (or CO_2-N_2(v)) in synthetic hydrates, with an emphasis on the impact of CH_4 hydrate formation conditions (e.g. driving force Δp) on the subsequent exchange reactions. Different driving forces Δp are utilized and show that the exchange kinetic is improved by a factor of ~3 when the exchange is performed with low Δp CH_4 hydrates, for which there is a higher relative amount of free H_2O(liq) (277 K); the kinetic is further improved when stirring is applied. Isobaric CH_4 hydrates exhibit a fast primary hydrate dissociation and CH_4 release, followed by a slower exchange kinetic, possibly limited by solid-state exchange diffusion or secondary CO_2-rich hydrate formation within the stability field of CH_4 hydrates. Upon exposure to a mixed CO_2-N_2(v) gas stream, secondary hydrate production is governed by the effective Δp remaining after dissolution of the gas mixture, and results in an even slower exchange reaction rate. These results may help optimizing recovery processes in field trial experiments, where both hydrates and liquid water coexist, and aid in predicting the risk of geo-hazards induced by unstable secondary hydrate formation. Furthermore, the exchange kinetic dependencies highlighted here are important as they affect the overall energy efficiency and energy cost of CH_4 recovery processes in gas hydrate field trials.

Keywords: Kinetic; Thermodynamic; Gas hydrate; CH_4-CO_2 replacement technology; CO_2 capture, Raman spectroscopy

1. Introduction

Carbone dioxide (CO_2) is the most important anthropogenic greenhouse gas and, as such, is one of the main contributors to global warming [1]. Anthropogenic CO_2 emissions result principally from the burning of fossil fuels (coal, oil, or gas) in industries, with thermal power plants being important emitters (up to 85 % of total anthropogenic CO_2) [2]. Developing alternative energy solutions (i.e., nuclear, biomass, solar energy, etc.) is of great interest to support the energy transition; however, the current alternatives still cannot fully supplant fossil fuel energy to meet the growing worldwide energy demand, and the use of non-fossil resources would further result in large technologic disruptions of the existing energy supply infrastructures. Natural gas (methane, CH_4) has been marked for years as a "bridge fuel" between conventional energy sources (i.e., fossil fuel) and alternative energies, with a transition period for the energy market estimated to span over more than 50 years [3]. Recently, natural gas hydrates (i.e. CH_4 molecules trapped within a crystal structure of water molecules), which are present in large amounts in offshore marine sediments and under the permafrost in the Arctic region, have received considerable attention as a promising medium for natural gas production. Different approaches such as depressurization, as well as thermal and chemical stimulation (hydrate chemical inhibitor injection [4], [5]), have been tested to recover

methane in natural gas hydrates, not only in laboratory studies but also in field trials [6–8]. However, complex issues still remain to be solved, such as the safe and efficient methane production from hydrates while making the process economically advantageous [3]. Currently, one promising approach is a chemical stimulation method, whereby CO_2 gas is injected into hydrate-bearing sediments. The underlying principle of this technique is based on the infusion of CH_4 clathrate hydrates with CO_2 gas (or flue gas, typically a CO_2-N_2 gas mixture), which results in CH_4 extraction from the clathrate hydrate structures and subsequent CO_2 capture and storage in the same structures. From a global carbon cycle perspective, this CH_4-CO_2 gas exchange process appears particularly favorable and represents a great potential for sustainable developments with industrial considerations. As to the sediment stratum stability during this process, the formation of CO_2-mixed hydrates alongside the dissociation of natural hydrates consumes water molecules and consolidates the sand bed released upon dissociation, which allows CH_4 exploitation from natural gas hydrates to be considered as a relatively safe method when suitable *p-T* conditions are met to concomitantly form mixed hydrates. While the past two decades of investigations evidenced many factors possibly affecting the reaction and subsequent CH_4 recoveries, the results of these studies principally agreed upon the two following observations. First, the CO_2 phase exerts an important influence on the exchange reaction, whereby the use of denser CO_2 phases (liquid and supercritical) or CO_2-based gas mixtures results in higher CH_4 recoveries. Second, the initial water phase strongly influences CH_4 recovery, as evidenced by the greater recovery yields obtained when powdered ice particles of specific size distribution are preferred as a starting mixture over large ice particles or even bulk water [9]. However, exchange processes conducted under conditions that both maintain the initial hydrate morphology and form a mixed hydrate (i.e., conditions which do not lead to CH_4 recovery by hydrates dissociation alone) should be preferred for a sustainable development of the technique.

Natural gas hydrates are known to crystallize into cubic structure I (sI), cubic structure II (sII) and hexagonal structure H (sH) [10]. The three structures are formed by a total of five different water cavities referred to as 5^{12}, $5^{12}6^2$, $5^{12}6^4$, $5^{12}6^8$, and $4^35^66^3$ [10]. A given hydrate structure is typically determined by the size and shape of the guest molecule, with the guest-to-cavity-size ratio rule indicating the preferential presence of the guest molecule in a specific cage type [10]. Simple guest molecules like CO_2 and CH_4 are known to usually crystallize into clathrate sI, with a unit cell containing 46 water molecules organized into two small (SC, 5^{12}) and six large (LC, $5^{12}6^2$) cages. In contrast, N_2-hydrates are known to form sII at low temperature and moderate pressure, and thus the unit cell contains 136 water molecules with 16 SC (5^{12}) and 8 LC ($5^{12}6^4$) [11,12]. Mixed CO_2-CH_4 hydrates are known to form sI [13], while mixed CO_2-N_2 hydrates form mainly sI in a wide composition range (> 2% CO_2) [14].

Since the pioneered work of Ohgaki et al. [15] and Hirohama et al. [16], early lab-scale investigations primarily focused on the feasibility of the CH_4-CO_2 exchange process within CH_4 hydrates. Gas replacement experiments were conducted with pure water (bulk or ice particles) and CH_4 hydrates produced by different methods were analyzed with different techniques to both determine the exchange kinetics and optimize the swapping process with respect to the recovery rate of methane (see for e.g. Komatsu et al., 2014 [17] and references therein for review). Considering the guest partitioning in an equilibrated CH_4-CO_2 mixed hydrate system at 280 K, Ohgaki et al. [15] showed that the CH_4-CO_2 replacement process in gas hydrates is thermodynamically favorable, as CO_2 hydrates are more stable than CH_4 hydrates [15]. Furthermore, the recovery of CH_4 from the parent hydrate was investigated upon liquid CO_2 injection under temperature and pressure conditions of 274-277 K and 4-5 MPa, respectively [16,18]. Starting from ~31 mol of water, about ~24 mol of water was subsequently converted into CH_4 hydrate, while ~7 mol of the remaining free water was transformed into CO_2-hydrate. In addition, about 12.5% of the parent CH_4 hydrate phase was further transformed into CO_2 hydrate after 800 h of reaction [16]. Thus, it was presumed that the low conversion rate resulted from the rapid formation of interfacial (gas-solid) mixed CO_2 hydrate, hence inhibiting the mass-transfer of CO_2, CH_4, and/or H_2O. More recently, Lee et al. [19] investigated CO_2-CH_4 exchange mechanisms starting from CH_4 hydrates (268 K, 21.5 MPa) prepared from ice particles

(5-50 μm and ~100 μm) in porous silica gel. They observed by NMR spectroscopy the slow exchange reaction kinetics of CO_2 at both 268 K and 270 K (at P = 5.8 MPa, i.e. with liquid CO_2), with a reaction still incomplete after 30 h, and determined a conversion rate constant of $k \sim 4.2 \times 10^{-5}$ s^{-1}. In contrast, they observed that the guest replacement reaction is completed in less than 5 h when CH_4 hydrates are exposed instead to CO_2 gas at 270 K (rate constant $k = 1.7 \times 10^{-4}$ s^{-1}). In addition, the conversion rate was observed to drop by a factor 3 when starting from CH_4 hydrate particles of ~100 μm diameter. The authors established a CH_4 recovery yield of 50 %, i.e. half of the total CH_4 present in the initial hydrate was recovered from this exchange reaction. Moreover, the produced hydrate phase exhibited a CO_2/CH_4 ratio of ~1, i.e. contained less CO_2 than expected from the theoretical estimation (CO_2/CH_4 ~1.8) [19], which suggested that the exchange reaction was limited by considerations other than thermodynamics. In addition, Ota et al. and Yoon et al. [20–23] thoroughly investigated the CH_4-CO_2 replacement reaction using material balance calculations and in-situ Raman spectroscopy with optical high pressure cells. Specifically, Yoon et al. [20] obtained 100% CH_4 recovery in 150 h (with a 60-40 partitioning for exchange and hydrate melting, respectively, at 278 K and 3 MPa), while only 10% of CH_4 was replaced in 20 h under less favorable conditions (CO_2 pressure of 0.8 MPa and 253 K), when pure CH_4 hydrate particles (no unreacted ice) of 100 to 250 μm were used during the exchange. Alternatively, Ota et al. [19], [20] applied a fugacity-based kinetic model to describe the reaction as a two-step process: (step 1) CH_4 hydrate dissociation, characterized by the rearrangement of water molecules, followed by (step 2) CO_2 (mixed) hydrate formation, whereby CO_2 molecules actively diffuse within the hydrate phase. The authors obtained CH_4 recovery yields ranging between 15 and 38%, depending on the starting CO_2 fluid phase and p-T conditions. Specifically, the authors suggested from their Raman and NMR analyses that the replacement of CH_4 by CO_2 molecules occurred in a majority of the $5^{12}6^6$ LCs, which would require the disruption of the whole lattice, as they are predominant in sI structures. Therefore, the authors proposed that the decomposition of both LCs and SCs is followed by the reformation of SCs with, however, preferential CH_4 entrapment [19,23].

Many natural gas hydrates investigations focused on the optimization of CO_2 injection conditions to increase CH_4 recovery rate. For instance, Zhou et al. [24] examined CO_2 injection conditions and showed that the most efficient methane recovery scenario consisted in injecting liquid CO_2 (at 281 K, 5 MPa) to create a p-T environment outside the stability zone of CO_2 hydrates and allow geotherm pressure conditions to be reduced by a depressurization method. Injection of liquid CO_2 was also investigated by Lee et al. [25] at 10 MPa starting from small methane hydrate particles (75-90 μm or 125-150 μm). The resulting exchange process was described by a combination of Avrami and shrinking core models [25,26], the former describing the initial reaction stage of the hydrate film covering the decomposed ice particles and the latter the diffusion through the hydrate film. However, the CH_4 recovery rate obtained by such a replacement was shown to be low (around 15-20 % in 115 h) [25] compared to that produced from dissociated hydrates (with no exchange) (~80-85%). Schicks et al. [27] further investigated CH_4-CO_2 substitution using Raman spectroscopy on small methane hydrate particles (ice particles of size < 10 μm) and estimated the CH_4 recovery rate to be at most 50 % in 115 h (exchange conditions of 3.2 MPa and 274 K), which is much less efficient than what was reported by Lee et al. [19] (50% in 5h). Schicks et al. evidenced several influencing factors that could account for that difference, such as the distinct chemical potential between the hydrate phase and the surrounding phase, the surface area of the particles, and the mobility of the guest molecules [27].

While laboratory works on exchange reactions continue to be published, literature results vary significantly with respect to the experimental conditions (in terms of hydrate formation procedures, replacement conditions, monitoring techniques) and so does the exchange performance. Nevertheless, recent progresses in the identification of key factors influencing the replacement kinetics through computational investigations showed that the rapid initial reaction stage may not be inter-cage exchange but instead full destruction and reconstruction of the interface leading to a heterogeneous guest composition [28,29]. This step is triggered by the sudden change in chemical potentials and equilibration of water and guest components between the methane hydrate and the injected fluid. Thus the penetration depth of CO_2 depends on several factors and was estimated to be ~10 μm or

higher in the methane hydrate crust [30,31]. In this context, the addition of less favorable gas hydrate formers in the injection fluid, such as H_2 [30] or N_2 [31], [34], was predicted to increase the reaction volume and artificially improve CH_4 recovery via destruction/re-formation of the hydrate [31]. While this latter method may be applicable, it could counterbalance the beneficial effects of solid-state exchange in maintaining sediment integrity in natural systems. Regarding the destruction/re-formation step at the hydrate surface, this view encountered controversies in the literature and spontaneous replacement without melting has been reported several times in CO_2-CH_4 systems both from experiments (e.g. [33], [35], [36]) and computational simulation [37]. Concerning the slow process resulting in the formation of a mixed-hydrate (step 2), an elaborated mathematical model describing the non-equilibrium migration of guests through the host lattice was developed using the "hole-in-cage" permeation scenario to account for the binary diffusion in gas hydrates of structure sI [31]. This model has been validated using kinetic exchange data in CH_4-CO_2 systems [30]. Such a description of permeation using molecular-scale mechanisms could well contribute to reliably predict methane production rates needed for the calculation of the economic balance.

Exchange processes in porous media and saline environments have also gained recent interest [24,38–42]. The aim is to improve CH_4 recovery by investigating different parameters such as water saturation in sediment analogs, salinity, sediment composition, etc. Although no clear trend is yet established, it was reported that open CO_2 flow configurations typically resulted in higher recoveries. By varying CO_2 injection conditions in porous media, several parameters influencing the exchange kinetic could be identified, such as the injection temperature, CO_2 injection rate, excess water in the sediment, etc [43–46]. While the replacement by CO_2 is generally low, CH_4 production could be increased by large-scale hydrate dissociation, likely at the expense of sand bed integrity. These results highlight the necessity to determine a comprehensive optimization procedure including a thorough examination of the impacts of all influencing factors on the exchange kinetic.

Investigating the replacement kinetic between CH_4 and CO_2 (or CO_2-based) gas is of fundamental interest for the understanding of the underlying micro-mechanisms involved, which need to be harnessed in order to improve the exploitation efficiency of methane. However, most of the studies so far have been focusing on optimizing CO_2 injection conditions without considering the phase partitioning or equilibrium state of the parent CH_4 hydrate. This lack of proper characterization or consideration of the initial CH_4-hydrate/liquid water/ice template greatly contributes to the scattering and sometimes apparent discrepancies across literature studies addressing the kinetic. In contrast, we investigate here the exchange kinetic between CH_4 and CO_2 (or CO_2-N_2) in synthetic hydrates, and stress the importance of considering the impact of CH_4 hydrate formation conditions on the subsequent exchange reactions as they exert an impact on the overall energy efficiency and energy cost of CH_4 recovery processes and could aid in identifying the best locations where these parameters are met in gas hydrate field trials. The CH_4 hydrate production rate is varied by tuning the driving force (Δp) applied at the onset of the hydrate synthesis. Specifically, different sets of experiments are performed to generate methane hydrates with distinct methane hydrate to free water (gas or water saturated) ratios (estimated by mass balance calculations) and different cage occupancies. The reaction products are then exposed to either CO_2 or (CO_2-N_2) gas injected at fixed p,T conditions. The exchange kinetic is monitored at constant volume in our new experimental hydrate set-up, working either in batch or semi-batch mode, and from which quantitative estimates of the overall kinetic can be derived. In addition, different factors likely driving the overall replacement reaction kinetic are investigated: stirring conditions and temperature at which the exchange is conducted. In parallel, Raman spectroscopy is sporadically applied to confirm the nature, structure, and composition of the reaction products.

2. Materials and Methods

2.1. Apparatus Description

The novel experimental setup used in this study is depicted in Figure 1. It consists of a batch reactor encompassing temperature, pressure, and Raman probes, to which are connected a syringe injection pump, a gas filling pumping station, and a vacuum pump.

The batch reactor comprises a custom-built 8.48 mL stainless steel cylindrical reactor with mechanical stirring (30 N.cm) and heating/cooling capabilities (Top Industrie). A syringe pump PU-2080 (JASCO) is used to measure the volume of the reactor. The stainless steel reactor is surrounded by a cooling jacket connected to a RP-855 thermostatic bath (Lauda) filled with an aqueous solution of 30 % glycol, which controls the reactor temperature between 243 K and 303 K. The stirrer consists of a pair of stainless steel two-blade impellers positioned at the top and middle of the reactor chamber. The stirrer is magnetically driven from 0 to 1500 rpm (rotation per minute). Pressure in the reactor is monitored using a high-pressure transducer PA33X (0-20.00 MPa, ±0.01 MPa) (Keller) and the temperature is measured via a K-type thermocouple (±0.5 K). Pressure and temperature variations are continuously recorded on a data logger (Graphtec GL-240). The stainless steel reactor is sealed at the top using a pressure-proof optical window, through which in-situ real-time Raman measurements can be performed using a HR-1000 spectroscope with a 600 grooves/mm grating (entrance slit width adjusted at 150 μm) coupled to a SuperHead fiber probe (Horiba) to reveal the composition of both the gas and hydrate phases.

The reactor and gas inlets are pumped out using a primary vacuum pump. De-ionized water is introduced to the reactor (Option Q, Purelab ELGA, with a resistivity of 18.2 MΩ.cm). Methane (CH_4) gas (99.9%) is injected into the reactor through a high-pressure valve. Pure CO_2 (99.995%) or binary gas mixtures CO_2:N_2 (20:80 mol:mol, ±5 % relative) (Air Liquide), for which exchange processes with CH_4 are studied, are injected into the reactor either directly through a high-pressure valve or using a syringe pump (PMHP50-1000, Park House Healthcare).

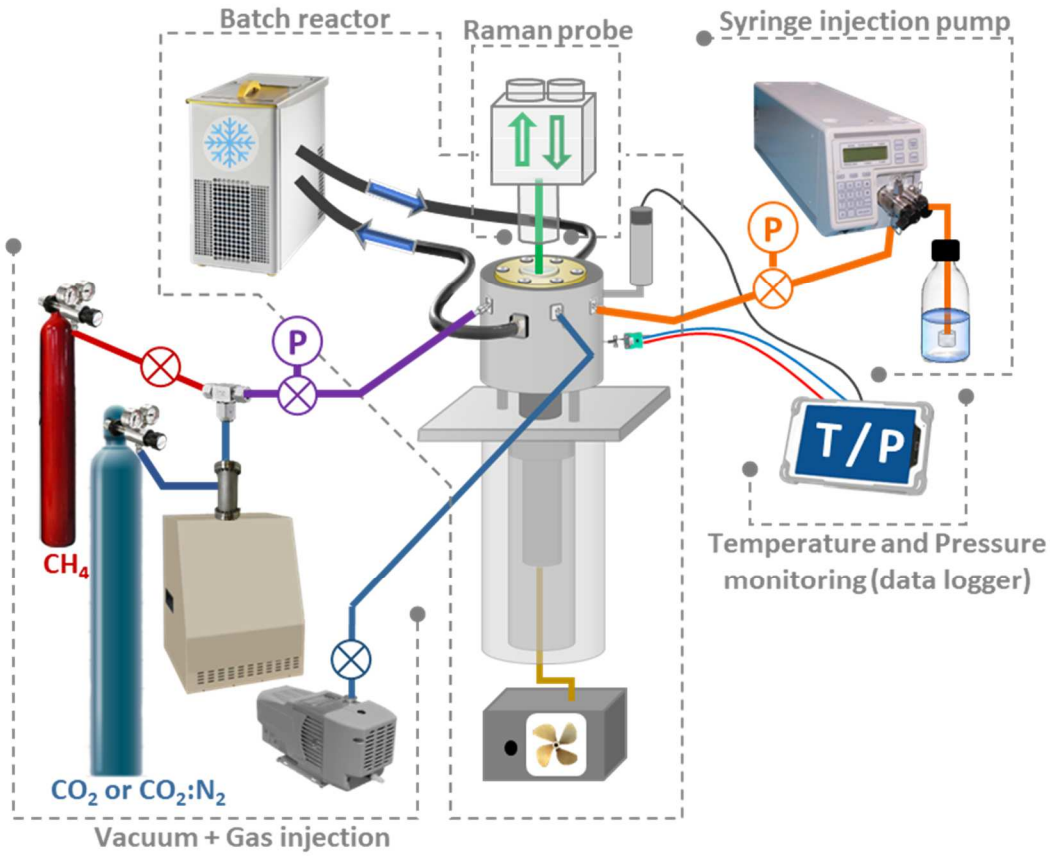

Figure 1. Experimental set-up. The batch reactor with mechanical stirring and cooling/heating capabilities is connected to both a temperature and a pressure probe. The reactor chamber is analyzed using a Raman fiber head. Crossed circles represent valves and P pressure gauges.

2.2. Experimental Procedure

2.2.1. Apparatus Validation

In order to validate our new setup for hydrate formation and check the robustness of the associated experimental protocols, we first investigated the equilibrium dissociation points of pure CH_4 and CO_2 systems in the temperature range of interest (~273-286 K, Figure 2). The reactor is filled with 3.8 mL of water prior to gas injection. CH_4 is then introduced at the desired pressure (~6 MPa or ~8.7 MPa) in the reactor and the system is cooled down to a temperature below the anticipated hydrate formation temperature (~277 K). Hydrate nucleation and growth are monitored by following both the system pressure and temperature in a water-saturated environment (i.e., gas limited). Once the pressure reaches a steady-state, the reactor temperature is elevated stepwise until complete dissociation occurs. Figure 2 compares our experimental data points with other experimental data sourced from the literature for pure CH_4 and CO_2 hydrates [47]. Our experimental data points (dissociation points) are collected at each temperature step and are in good agreement (within 4%) with literature results, which validates our experimental set-up for hydrate formation and monitoring.

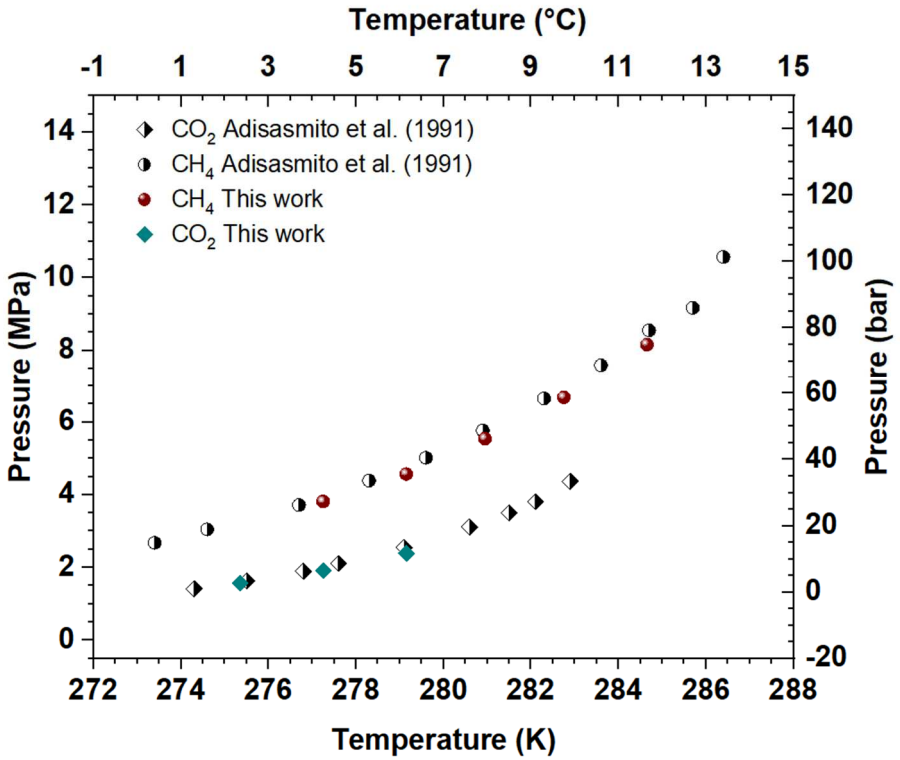

Figure 2. Experimental equilibrium data points obtained for pure CH_4 and pure CO_2 gas hydrates compared with literature data from from Adisasmito et al., 1991 [47]..

2.2.2. Methane Hydrates Formation Protocols

Prior to the experiment, the stainless steel reactor is scrubbed using de-ionized water and cleaning tissues. The air is then pumped out of the reactor and the gas inlets, and primary vacuum is maintained for 10-20 min. Once a base pressure of 10^{-1} mbar is reached, the temperature in the reactor

is set to 284 K. Then, 3.8 mL of de-ionized water is injected into the reactor via a syringe. Stirring of the reactor is started immediately upon water injection at a rate of ~1000 rpm and continued for about 9 minutes until both the pressure and temperature are stable. Stirring is momentarily stopped as the reactor is pressurized with CH_4 gas and resumed immediately when the desired pressure load is reached (~6 or ~8.7 MPa depending upon the experiment). Figure 3 illustrates the experimental pathways of experiments I to IV projected onto a *p-T* diagram along with Hydrate-Vapor-Liquid Equilibrium (HVLE) curves of CH_4-H_2O, CO_2-H_2O, N_2-H_2O, and CO_2:N_2-H_2O. Two setup configurations are utilized to form CH_4 hydrates: batch and semi-batch. In experiments I to III, and V the reactor is isolated (i.e., valves are closed – batch configuration) and the system is left to equilibrate for about 20 min at 284 K (step 1). It works in a water-saturated (gas-limited) configuration. In contrast, in experiment IV, the reactor is configured for open gas flow (semi-batch configuration), whereby the CH_4 gas cylinder applies a constant pressure of 8.7 MPa. This system works in a gas-saturated (water-limited) configuration. An equilibration time of about 20 min at 284 K is also allowed in this procedure (step 1). In all experiments (I to IV) the temperature is then decreased to 277 K with a cooling rate of 5 $K.min^{-1}$ which triggers the crystallization of CH_4 hydrates (step 2). After a pressure drop of 2-4.5 MPa (compensated for in the isobaric experiment IV, step 2′), equilibrium is reached at about 4 MPa (8.5 MPa for experiment IV) when pressure only varies within 0.1 MPa over time (step 3). The equilibration time lasts either 1 to 2 days (depending on the initial pressure) for experiments I to III, or up to 7 days for the isobaric experiment IV. Experiments I to IV provide a variety of formation pathways for CH_4 hydrates, which influence the thermodynamic parameters and can be used to assess the effect of gas-hydrate conversion (CH_4-hydrate loading) and cage occupancy upon the CH_4-CO_2 and CH_4-CO_2:N_2 exchange processes yet to occur.

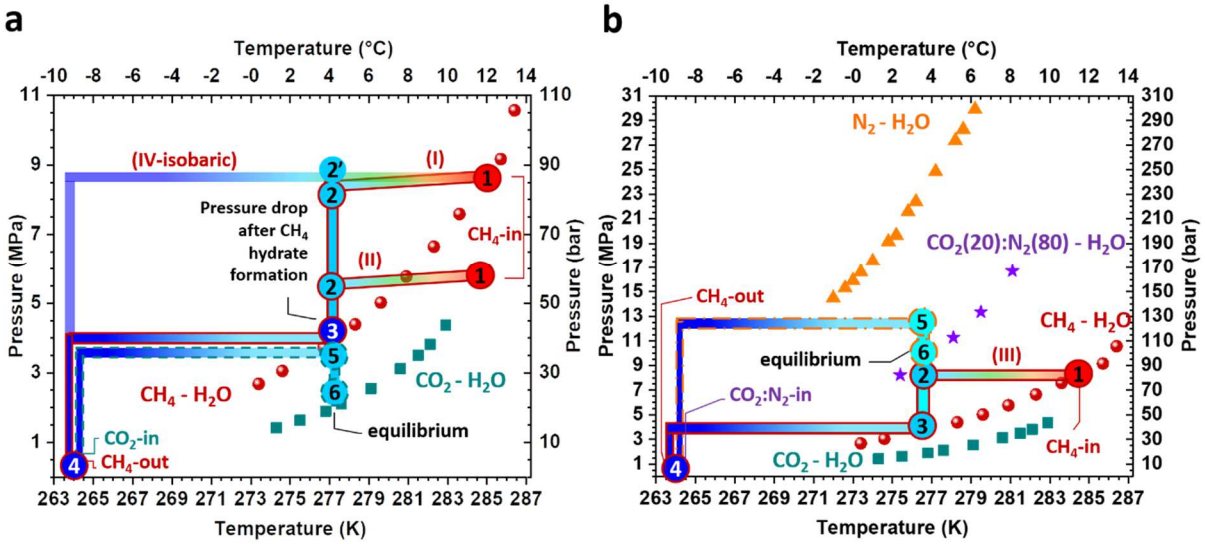

Figure 3. Experimental pathways (I, II, III, and IV) followed for CH_4-CO_2 (a) and CH_4-CO_2:N_2 (b) exchange experiments projected onto a *p-T* diagram. Pure CO_2 (squares), CH_4 (circles), [47] and N_2 (triangles) [48] clathrate hydrates equilibrium curves are depicted along with that of a mixed CO_2(20):N_2(80) clathrate hydrate (stars) [49]. Experimental steps (circled numbers) followed in experiments I to IV are shown: steps 1→3 CH_4 hydrates formation, step 4 gas replacement whereby residual CH_4(v) is purged out and CO_2(v) or CO_2:N_2(v) is introduced, step 5→6 exchange reaction between CH_4 hydrates and CO_2 or CO_2:N_2 gas and system equilibration.

2.2.3. Exchange Processes with CH_4-CO_2 and CH_4-CO_2/N_2

Exchange processes are investigated for experiments I to Va. Note that experiment Va is not displayed in Figure 3 for better visibility; this experiment will be used later on for comparison purposes. The difference between the ensemble of experiments I to IV and experiment Va results from the

temperature at which step 4 is realized (Figure 3). Step 4 is initiated when the pressure of CH_4 remains stable within 0.1 MPa over several hours. Then, two distinct temperature protocols are followed for the gas replacement (purge of residual CH_4(v) and injection of CO_2(v) or CO_2:N_2(v)) (step 4). The temperature is either decreased to 264 K (protocol 2: experiments I to IV) or maintained at 277 K (protocol 1, experiment Va), whereas the mechanical stirring is stopped during this action in both protocols to avoid premature CH_4-hydrate dissociation. Then, for protocol 2, the reactor temperature is increased back up to 277 K and stirring is resumed only when its effect on the exchange process is studied. Accordingly, experiments I to IV can be further broken down into two categories: when exchange experiments are stirred (experiments Ib, IIb, IIIb – stirring 'on' during the exchange), and when they are not (experiments Ia, IIa, IIIa and IVa – stirring 'off' during the exchange). These experimental specificities are summarized in Table 1. In addition, mass balance calculation is used to evaluate the mole numbers of CH_4, CO_2, N_2, and H_2O in the reactor for steps 1 and 3 (start and end of CH_4 hydrate formation, respectively), and 5 and 6 (start and end of the exchange reaction, respectively) for each of all eight experiments (Table 1). Further details about the gas, liquid, and/or hydrate composition during both CH_4 hydrate formation and exchange processes can be found in supplementary material.

Table 1. Experimental conditions for CH_4 hydrate formation and subsequent exchange processes. Exponents 0 and f refer to the initial and final step, respectively, delineating CH_4 hydrate formation (steps 1→3) and exchange processes (steps 5→6). *p* stands for the total pressure in the reactor, *n* is the mole number and *X* the gas component added for the exchange, with CO_2:N_2 at a composition of 20:80. Mole numbers are derived from mass balance calculations (see supplementary material). The theoretical equilibrium pressure (*Eq.* p_f) of step 5→6 is calculated with *CSMGem* [10] using total feed mole numbers and temperature as inputs.

	Step 1 → 3: CH_4 hydrate formation							**Step 5 → 6: CH_4 ↔ X exchange**							
	Exp.	**Stir.**	p_1^0 **(MPa)**	$n(CH_4)h,f$ **(mmol)**	$n(H_2O)h,f$ **(mmol)**	$n(H_2O)liq,f$ **(mmol)**	p_3^f **(MPa)**	**Stir.**	**X**	p_5^0 **(MPa)**	$n(CH_4)v,0$ **(mmol)**	$n(CO_2)v,0$ **(mmol)**	$n(N_2)v,0$ **(mmol)**	p_6^f **(MPa)**	*Eq.* p_f **CSMGem**
Protocol 2	Ia	ON	6.37	5.4	31.5	179.7	3.89	OFF	CO_2	3.37	0.2	9.3	N.A.	2.04	2.34
	Ib	ON	6.01	4.7	26.8	184.6	3.84	ON	CO_2	3.42	0.2	9.6	N.A.	2.09	2.29
	IIa	ON	8.76	11.6	66.6	145.0	3.96	OFF	CO_2	3.71	0.2	9.3	N.A.	2.04	2.60
	IIb	ON	8.57	11.3	64.9	146.2	3.99	ON	CO_2	3.39	0.2	9.4	N.A.	2.48	2.59
	IIIa	ON	8.81	11.6	66.7	145.0	4.02	OFF	CO_2-N_2	11.91	0.2	6.0	23.8	9.70	6.22
	IIIb	ON	8.81	11.7	67.1	144.6	3.98	ON	CO_2-N_2	11.54	0.2	5.9	23.6	10.20	6.32
	IVa[1]	ON	8.70	N.D.	N.D.	N.D.	8.70	OFF	CO_2	3.72	0.2	10.8	N.D.	4.33	3.51
Protocol 1	Va[2]	ON	8.96	9.5	54.7	156.4	4.05	OFF	CO_2	4.06	0.2	12.6	N.A.	1.95	2.39

[1] Isobaric CH_4 hydrate formation. [2] Gas replacement made at 277 K (Protocol 1). N.A. stands for 'not applicable' to the experiments where only CO_2 exchange is considered. N.D. stands for 'not determined' and refers to the situation where the number of moles consumed cannot be evaluated precisely, such as for the isobaric experiment.

3. Results and Discussions

3.1. Initial CH_4 Hydrate Formation Conditions in a Stirred Batch and semi-Batch Reactor

In order to study the influence of CH_4 hydrate formation conditions on the exchange process, distinct initial CH_4 gas pressures (or driving force Δp) are used while cooling the resulting pressurized CH_4 gas – liquid water system from ~285 K to 277 K. The driving force Δp is varied from Δp ~ 5 MPa

(experiments II, III, IV-isobar) to Δp ~ 2.4 MPa (experiment I), which eventually results in distinct water to hydrate conversion ratios, with values by mass at step 3 of about 13-15 wt%, 30.7 wt%, and ~ 100 wt%, for experiments I, II-III, and IV, respectively. This means that different amounts of free water coexist with CH_4 hydrates at the end of the formation process and thus prior to the exchange with CO_2 (or CO_2-N_2) (Table 1). Additionally, pressures reached in only one day are very close to the end pressure target given at the HLV equilibrium (3.81 MPa at 277 K [47,50]), regardless of the CH_4 hydrate formation protocol. Upon longer reaction times (up to several days), no significant change in pressure is observed, the end pressure p_3^f falling within 0.8–5% relative deviation from the equilibrium pressure at HLV conditions.

The time evolution of CH_4 mole numbers in each of the 3 phases (hydrate (h), liquid (liq), and vapor (v)) during CH_4 hydrate formation is displayed in Figure 4a and 4b for experiments IIa and Ia, respectively. Molecules of CH_4 in the vapor phase (nCH_4(v)) are rapidly consumed within the first 2h (experiment IIa) or 8h (experiment Ia) of reaction, principally in the hydrate phase (steep decrease of nCH_4(v) and reciprocal increase of nCH_4(h), between (t_1^0+ 20min) and (t_1^0+ 20min) + 2h/8h, Figure 4a and 4b) and only marginally in the liquid phase. Moreover, the consumption of nCH_4(v) is significantly different between experiment IIa (high driving force Δp ~ 5 MPa) and experiment Ia (lower driving force Δp ~ 2.4 MPa), with twice as much of CH_4 molecules trapped in the hydrate phase in experiment IIa (~11.6 mmol) in comparison to Ia (~5.4 mmol) (Table 1). Accordingly, the amount of free liquid water available at step 3 in experiment IIa (145 mmol) is smaller than that in Ia (~180 mmol). Note that these results also apply to other experiments, where a greater amount of free liquid water remains at the end of experiments conducted at an initial lower driving force. Moreover, as a constant pressure is applied during the whole isobaric experiment IVa (until the gas flow needed to maintain the pressure becomes negligible), we consider that no free liquid water exists at step 3, all of it being converted to CH_4 hydrates in such a water-limited (gas saturated) environment.

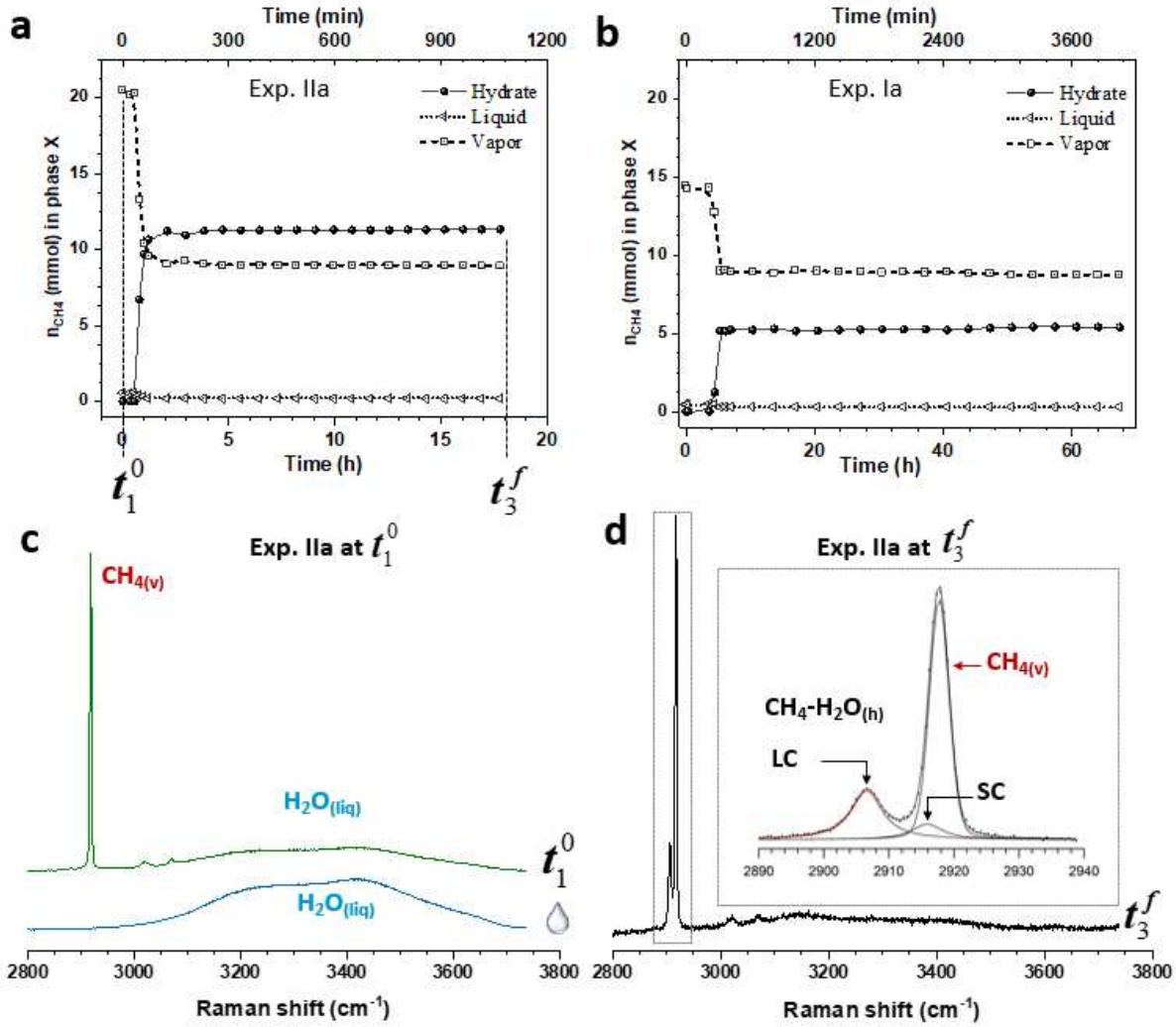

Figure 4. Time evolution of CH_4 mole numbers in each of the 3 phases (hydrate, liquid, and vapor) for experiments IIa (a) and Ia (b). Raman spectra acquired at the beginning (t_1^0) and the end (t_3^f) of steps 1 and 3 of experiment IIa, respectively, are presented in panels (c) and (d). The spectrum acquired at t_1^0 (c) shows the signatures of CH_4(v) and liquid water. A Raman spectrum of pure liquid water is plotted for comparison. The spectrum acquired at t_3^f (d) is enlarged and shows the specific signature of CH_4 hydrates (CH_4(h)), from which can be inferred the contributions of their large cages (LC) and small cages (SC).

The partition of CH_4 molecules into the gas, hydrate, and liquid phases can also be inferred from Raman measurements. Our Raman analysis performed during experiment IIa is displayed in Figure 4c and 4d. Raman spectra are collected at two specific kinetic stages: t_1^0 (Figure 4c), time at which ~8.8 MPa of CH_4 has been injected into the reactor containing liquid water (step 1, 284 K) and t_3^f (Figure 4d), time associated with complete (i.e. no more pressure change) CH_4 hydrate formation (step 3, i.e. after ~18 h at 277 K and an end pressure of ~3.9 MPa). At t_1^0, the Raman spectrum exhibits the characteristic signatures of pure methane gas (C-H stretching ν_1 at ~2918 cm^{-1}, ν_3 at ~3020 cm^{-1} and overtone $2\nu_2$ at ~3070 cm^{-1}), [51] and pure liquid water (O-H spectral region). Note that the Raman spectrum of pure liquid water was collected prior to CH_4 injection and is also shown in Figure 4c for comparison purpose. The Raman spectrum acquired at t_1^0 indicates that no CH_4 hydrate is detected upon CH_4 injection, which confirms the induction time observed in Figure 4a. Time t_3^f corresponds to a steady-state where both the CH_4 hydrate and CH_4 gas phases coexist with p-T conditions close to the equilibrium (Figure 4d, Table 1). Accordingly, the Raman spectrum of the C-H spectral region, enlarged in the inset of Figure 4d, no longer shows a single peak but instead a larger feature that can be further deconvoluted into three bands: the ν_1 C-H stretching of CH_4(v) at ~2918 cm^{-1} and a pair of

two bands pointing at ~2906.5 cm^{-1} and ~2916 cm^{-1}, which are characteristic of CH_4 molecules trapped in the LC and SC of clathrate structure sI, respectively, in agreement with previous investigations [51],[52]. Structure sI is deduced from the two Raman signatures characteristic of the CH_4 hydrate (i.e. LC and SC), which yield an integrated intensity ratio (I_{LC}/I_{SC}) of ~ 3.2, which is close to that expected in the cubic structure sI with full occupancy of all cages ($6 \times 5^{12}6^2 + 2 \times 5^{12}$). Thus, assuming the LC are fully occupied by CH_4 molecules (100% occupancy [53]), the cage occupancy of the SC is calculated to be ~94 % in our sample.

As the total pressure of CH_4 in the reactor is monitored as a function of time during the hydrate formation process, kinetic curves can be derived from all experiments but IV-isobaric. The kinetic curves can then be fitted using a simple exponential decay function, from which can be retrieved the average rate constant characteristic of CH_4 hydrate formation:

$$p_{fit} = \left(p_{0,fit} - p_{f,fit}\right) e^{-kt} + p_{f,fit}\,, \quad (1)$$

where p_{fit} is the fitted pressure value, $p_{0,fit}$ and $p_{f,fit}$ are adjustable parameters corresponding to the initial and final pressure values at time zero and infinity, respectively, k is the rate constant of the reaction. The rate constants derived from our kinetic curves are listed in Table 2. These rate constants characterizing CH_4 hydrate formation allow for qualitative comparisons across our experiments to reveal the influence of the driving force (Δp) on the reaction kinetic. Our results show that CH_4 hydrates produced at high driving force (Δp ~ 5MPa) in experiments II, III, and Va exhibit consistently higher rate constants (~ 9-12 $\times 10^{-4}$ s^{-1}) than those produced at lower driving forces (Δp ~ 2.4 MPa) such as in experiment I (~4-6 $\times 10^{-4}$ s^{-1}). Comparisons with other rate constants found in the literature for the same reaction can be undertaken while keeping in mind that CH_4 hydrate formation conditions influence the formation kinetic (as shown here) and therefore are just qualitative. Lee et al., 2003 [19] obtained a rate constant of ~0.15 $\times 10^{-4}$ s^{-1} at 21.5 MPa and 270 K for CH_4 hydrate produced from powdered ice in silica pores whereas Cha et al., 2015 [33] reported a higher rate constant of ~8 $\times 10^{-4}$ s^{-1} using a similar protocol but different formation conditions with CH_4 hydrates produced at 276 K and 14 MPa in silica pores. In our study, the starting material is water and all experiments are stirred during CH_4 hydrate formation.

Table 2. Rate constants for methane hydrate production. As the pressure is constant in isobaric experiment IVa, its rate constant could not be inferred from this equation.

Exp.	k (s^{-1}) (x 10^{-4})	Std. Dev. (x 10^{-4})
Ia	6.49	0.03
Ib	4.11	0.01
IIa	9.97	0.03
IIb	11.90	0.04
IIIa	11.4	0.1
IIIb	9.42	0.03
IVa	N.A.	N.A.
Va	12.25	0.02

3.2. Influence of Gas Replacement Temperatures: 277 K vs 264 K.

Once CH_4 hydrates are formed, an intermediate step (step 4) involving CH_4(v)–CO_2(v) (or CH_4(v)–CO_2:N_2(v)) replacement is necessary before the exchange can take place. The temperature at which occurs this gas replacement is either 277 K (protocol 1, experiment Va) or 264 K, the latter being immediately increased back to 277 K once the replacement is complete (protocol 2, experiments I to IV, Table 1 and experimental section 2.2.3). The effect of this gas replacement temperature on the exchange kinetic is investigated comparing steps 5→6 of experiments Va and IIa, which followed the

same CH_4 hydrate formation pathway (p_1^0 ~ 8.8 MPa, driving force of Δp ~ 5 MPa) but differ in their gas replacement protocol (step 4). Figure 5 shows the variation of total reactor pressure with time for experiments Va and IIa during steps 5→6. Note that the two experiments are at 277 K during these total reactor pressure decays. At t_5^0, the gas phase in the reactor is mainly composed of CO_2 gas, with only a residual partial pressure of CH_4(v) of ~0.1 MPa (the origin of the abscise (at t_5^0) has been set to 0 for clarity in Figure 5). The two kinetic curves exhibit distinct striking features: a smooth (almost) continuous exponential-like decay (loss of ~1.8 MPa over ~20 h) is observed in experiment Va (protocol 1), whereas irregularities with several bumps in pressure appear in experiment IIa (protocol 2). Specifically, the whole pressure decay curve of experiment IIa can be further broken down into 2 distinct curves: first, a pressure drop of ~ 1.1 MPa within the first ~10 h, followed by a slower pressure decline (with a pressure loss of only 0.4 MPa over the next ~35 h) exhibiting several pressure bursts. Three distinct processes may be concomitantly at play to explain the variations observed on the pressure curves [54]. These processes are: i) CH_4 hydrate dissociation, ii) CO_2 dissolution in the remaining free liquid water and CO_2-rich secondary hydrate formation resulting from either CO_2 vapor – liquid water interaction or from CO_2 dissolved in liquid water, and iii) simultaneous gas exchanges within the hydrates, where a molecule of CO_2 replaces a molecule of CH_4 by shrinking core solid-state diffusion [31]. The impacts of these three phenomena on the total reactor pressure are very different. The dissociation of CH_4 hydrates greatly increases the reactor pressure. Solid-state gas exchanges produce additional slight pressure increases because CO_2 possesses a higher density than CH_4 in the vapor phase in our *p-T* conditions (considering a 1:1 replacement in our isochoric system) [55]. In contrast, CO_2 dissolution and CO_2-rich hydrate formation both result in significant and fast pressure drops. Therefore, the only processes explaining the pressure drops observed in both experiments (Figure 5) are mainly CO_2 dissolution and CO_2-rich hydrate formation from liquid water. Liquid water could have remained in the reactor from the incomplete CH_4 hydrate formation (as indicated by the mole number of liquid water calculated at the end of the parent hydrate formation process (step 3, Table 1), and also produced by the dissociation of the CH_4 parent hydrate (destruction-reconstruction processes of the hydrate). Accordingly, the total reactor pressure curve shape observed in Figure 5 for experiment IIa can be interpreted as follows: the first pressure fall corresponds to CO_2(v) dissolution in free liquid water and its subsequent slow diffusion within the liquid phase toward the hydrate particle interfaces to form secondary hydrates, whereas the small bumps appearing during the second and slower pressure fall correspond to the successive releases of CH_4 gas from the parent hydrate. Thus, the parent hydrate releases CH_4(v) to compensate for pressure losses induced by CO_2(v) dissolution and CO_2(v) incorporation into a secondary hydrate (forming pure CO_2 hydrate or mixed CO_2-CH_4 hydrate), eventually allowing the system to reach chemical equilibrium.

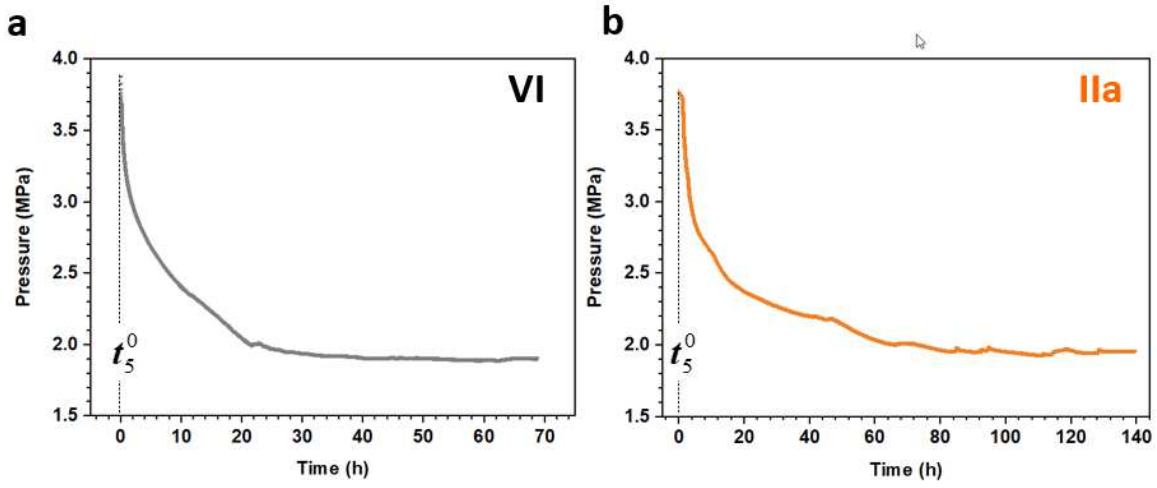

Figure 5. Total reactor pressure evolution during unstirred CH_4-CO_2 exchange processes of experiments (a) Va (protocol 1) and (b) IIa (protocol 2).

A simple exponential decay function can also be used to fit the total reactor pressure decay curves to provide rate constants characteristic of the secondary hydrate formation reaction for all experiments (Table 3). However, for comparison purposes, the total reactor pressure decay curves for experiments I to IV (protocol 2), which tend to show two-segment curves (steep fall followed by slow incline), need to be considered as a whole. Therefore, the resulting calculated rate constants constitute average rate constants describing the whole decay. The rate constant of experiment IIa (protocol 2) is found at ~0.16 $\times 10^{-4}$ s^{-1}, which is two times lower than that of experiment Va (~0.3 $\times 10^{-4}$ s^{-1}, protocol 1). This difference results from the temperature at which was performed the gas replacement (264 K and 277 K, for protocols 2 and 1, respectively), which eventually governs the amount of free liquid water available in the reactor. Specifically, we expect for reaction IIa (protocol 2) that the CH_4 hydrate phase remains well preserved during the gas replacement step (264 K) due to the self-preservation effect [56]. This would prevent significant CH_4 dissociation. Conversely, we expect for reaction Va (protocol 1) that an important part (if not all) of the CH_4 hydrate dissociates during the gas replacement step (due to the quick pressure release at 0.1 MPa and 277 K), and thus that free liquid water, possibly containing dissolved CH_4, is present in significant amount in the reactor. Therefore, the slower rate constant derived for experiment IIa with respect to experience Va likely results from CO_2 consumption (through dissolution and secondary hydrate formation) being impeded by the well-preserved CH_4 hydrate phase, in contrast to experiment Va, for which the higher rate constant describes a secondary hydrate formation process occurring more readily in presence of free liquid water.

In addition, the end pressure of experiment Va (p_6^f , Table 1) is closer to that of pure CO_2 hydrate (HLV equilibrium) at 277 K (~1.9 MPa, [47]) than is experiment IIa, which indicates that the secondary hydrate formed in experiment Va contains more CO_2 molecules than CH_4 molecules, as expected for secondary hydrates produced from free liquid water. These results demonstrate how the preservation of the primary CH_4 hydrate impacts the exchange reaction with CO_2. Note that such preservation effects have been macroscopically observed through a reactor window within a similar CO_2-CH_4-H_2O system [54].

The rate constants corresponding to the stirred experiments (Ib, IIb, IIIb) are significantly greater (one order of magnitude, Table 3) than their unstirred counterparts (Ia, IIa, IIIa) and, for most, become comparable to those obtained for pure methane hydrates, which were all formed with vigorous stirring. This result is expected as the stirring process facilitates CO_2 diffusion within the system in increasing the gas-hydrate particle interfaces renewal and mixing probability of the three phases (liquid, solid, vapor). Note that experiments III exhibit slower kinetic constants compared to their counterparts (experiments I and II). This may be due to the lower effective driving force remaining after dissolution of the CO_2-N_2 gas mixture; additionally, in contrast to experiments I and II, the exchange occurring in experiment III takes place in the stability domain of CH_4 hydrates, which may reduce CH_4 hydrates dissociation. While exchange rate constants may be similar between experiments, the composition of secondary hydrates is, however, expected to be different as the CH_4 hydrates systems are initially formed with different driving forces and/or experimental pathways.

Table 3. Kinetics of the gas exchange process corresponding to step 5→ 6 using Equation 1. The obtained fitted parameters are those described in Eq. 1.

Exp.	$p_{0,exp}$ (Mpa)	$p_{f,exp}$ (Mpa)	$p_{0,fit}$ (MPa)	$p_{f,fit}$ (MPa)	k ($\times 10^{-4}$ s^{-1})	Std. Dev. ($\times 10^{-4}$)
Ia	3.37	2.04	3.14	2.03	**0.522**	0.002
Ib	3.42	2.09	3.17	2.16	**4.37**	0.06
IIa	3.36	2.04	3.32	1.97	**0.1567**	0.0004

IIb	3.39	2.48	3.33	2.49	**1.94**	0.02
IIIa	11.91	9.7	10.15	9.63	**0.0175**	0.0001
IIIb	11.54	10.20	10.63	10.26	**0.175**	0.001
IVa[1]	3.72	4.33	4.87	3.48	**0.00235**	3×10^{-6}
Va	4.06	1.95	4.84	1.9	**0.2846**	0.0003

[1] Isobaric CH_4 hydrate formation.

3.3. Influence of the initial CH_4 Driving Force on the Exchange Process

The variation of total reactor pressure during the exchange process and the initial phase partitioning for experiments IVa, IIa, and Ia are depicted in Figure 6. Similar pressure decay trends, with yet different kinetics, are observed for experiments IIa and Ia, which differ in the driving force applied to form the primary CH_4 hydrate. We assessed before that the first abrupt pressure loss results from CO_2 dissolution and CO_2-rich hydrate formation from liquid water. In order to infer the relative involvement of these two processes, we calculate the maximum pressure loss that can result from CO_2 dissolution in the quantity of water available in the reactor, considering the fact that in favorable hydrate pressure conditions, the solubility of CO_2 is lower [57,58]. Consequently, maximum pressure losses of ~0.8 MPa and ~1 MPa for experiments Ia and IIa, respectively, can be imputed to CO_2 dissolution. Therefore, as these values are significantly lower than the observed pressure drops (~1.7 MPa in both experiments), this shows that CO_2-rich hydrates are indeed formed in both experiments and dissolution alone cannot account for the steep pressure loss.

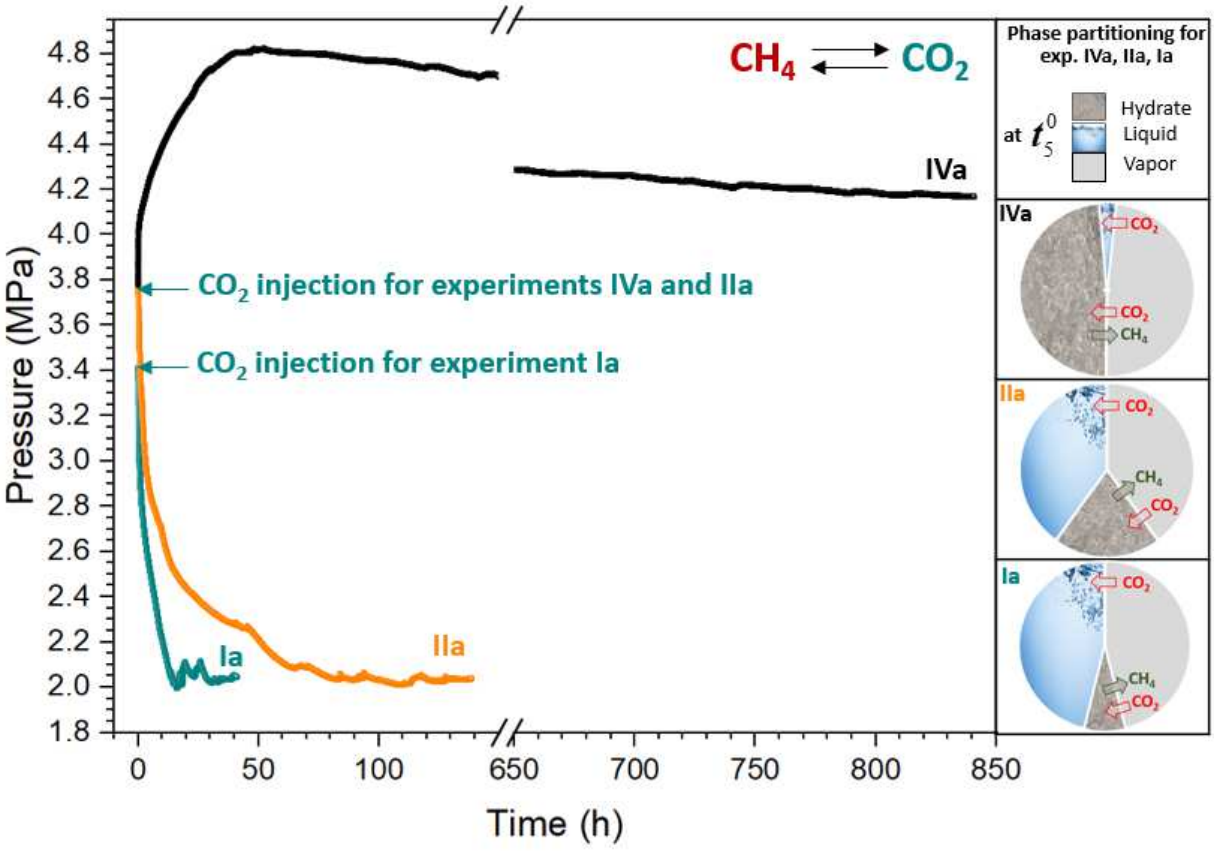

Figure 6: Pressure evolution with time during CH_4-CO_2 exchange experiments (stirring off) starting from three distinct CH_4 hydrates systems formed with different driving forces (exp. Ia vs IIa) or experimental pathways (exp.

IIa vs IVa-isobaric). The initial phase partitioning for the three experiments is schematically illustrated in the right-hand side column.

Figure 6 shows that experiment Ia exhibits a faster exchange kinetic (k ~ 0.5 × 10^{-4} s^{-1}) than that observed for experiment IIa (k ~ 0.16 × 10^{-4} s^{-1}, Table 3). Note that the initial CH_4 hydrate content prior to the exchange process is also smaller in experiment Ia compared to IIa, which also implies that the amount of liquid water available is greater in experiment Ia (Figure 6). As a consequence, the propensity for CO_2 absorption at the vapor-liquid interface is substantially larger, which results in a faster exchange kinetic for experiment Ia. In addition, it is possible that a distinct hydrate morphology exists for experiment Ia, which could favor secondary hydrate formation and/or exchange processes and impact the resulting kinetic [59].

When the initial conversion of water to CH_4 hydrate is very high, as in the isobaric experiment IVa (i.e., conversion almost complete, Figure 6), the total reactor pressure curve recorded during the exchange process exhibits a very different trend, starting instead with a significant increase (from ~ 3.8 to 4.8 MPa at 277 K) over a span of 50 h, with a 50 h-pressure toping above the HVLE pressure expected for the primary CH_4 hydrate [47]. This increase stems from primary CH_4 hydrates dissociation (solid-state exchange processes being too slow to account for this fast pressure increase [31]), which predominates in this experiment over CO_2 dissolution and secondary CO_2-rich hydrate formation. The system constituted of CH_4 hydrates pressurized with CO_2(v) is thermodynamically unstable because of the low chemical potential of CH_4(v) that forces the hydrate bulk to dissociate. Consequently, all independent intensive thermodynamic variables (i.e. *p*, *T*, and chemical potential) must be considered to establish when the equilibrium is reached and to evaluate the efficiency of an exchange in the long term [60]. Once the total reactor pressure in experiment IVa has topped ~ 4.8 MPa, the pressure starts decreasing and maintains this downward slope for over 35 days, exhibiting regular and very small pressure bursts along the way (Figure 6). The bursts may be assigned to remnant parent CH_4 hydrates dissociation and/or solid-state exchange reaction (diffusion), whereas the negative slope is characteristic of secondary CO_2-rich hydrate formation. A kinetic constant of 0.00235 x 10^{-4} s^{-1} was derived from this downward slope, which is about 2 orders of magnitude slower than those obtained for the second-segment curves of experiment Ia and IIa (after the initial pressure loss corresponding mainly to CO_2(v) dissolution, i.e. from 15 h and 50 h of reaction for experiments Ia and IIa, respectively). Note that the second-segment curves for experiments Ia and IIa exhibit pressure bursts much more pronounced than those observed in experiment IVa. The difference in exchange kinetics may originate from the fact that experiment IVa progresses in a *p*, *T* domain theoretically stable for CH_4 hydrates, resulting in very slow secondary CO_2-rich hydrate formation and CO_2 dissolution processes. The enrichment of the vapor phase in CH_4 molecules with respect to CO_2(v) is further confirmed by our Raman analysis (section 3.4.), which allows for the quantitative monitoring of the CO_2(v)/CH_4(v) ratio. A molecular CH_4:CO_2 1:1 exchange would have eventually slightly increased the total reactor pressure in contrast to what is observed here, where more CO_2 molecules leave than CH_4 molecules enter the vapor phase. To summarize, the gas exchange kinetic is driven by the initial CH_4(h)/H_2O(liq)/CO_2(v) partitioning and therefore depends greatly on the initial driving forces applied to produce the primary CH_4 hydrate and the experimental pathways followed to form both the primary and second hydrates.

3.4. Real time and in-situ Raman spectra for the identification of phases and cage occpuancy

Phase partitioning, hydrate cage occupancy, and their evolution with time during the exchange process are further monitored via Raman spectroscopy. Raman spectra portraying five snapshots in time (t_a-t_e) are recorded along the total reactor pressure curve and shown in Figure 7a-c. Raman signatures of both CO_2 and CH_4 hydrates (CO_2-H_2O(h) and CH_4-H_2O(h)) and those of the vapor phase (CO_2(v) and CH_4(v)) are acquired at the same position of the laser probe at different times (Figure 7b). Raw Raman spectra are further fitted using a set of Voigt functions from which can be derived the

clathrate structure and cage occupancy. This procedure is applied to all spectra discussed from here on. Two pairs of Raman peaks pointing at ~1275/1380 cm^{-1} and ~1284/1387 cm^{-1} are identified as CO_2-H_2O(h) and CO_2(v), respectively (Figure 7c). They are known to be caused by a Fermi resonance effect of the symmetric stretching mode (ν_1) (C-O stretching) and the overtone of the bending mode ($2\nu_2$) of the CO_2 molecule, whereby both peaks (~1284/1387 cm^{-1}) are a mixture of ν_1 and $2\nu_2$ [61] . These frequencies are consistent with literature values [14]. The C-H stretching region can be deconvoluted into three or four bands, with the signature of CH_4(v) observed at ~2919 cm^{-1} (C-H stretching ν_1), and those of CH_4-H_2O(h) at ~2906.2 cm^{-1} (LC) and ~2916.5 cm^{-1} (SC). The clathrate structure sI is deduced from the Raman band intensity ratio LC to SC (I_{LC}/I_{SC}) in CH_4-H_2O(h). This ratio evolves with time; it starts from an initial value of I_{LC}/I_{SC} ~3.2 observed at the end of CH_4 hydrate formation (i.e. at time t_3^f, Figure 4), and reaches ~2.5 at the end of the exchange reaction after ~140 h (time $t_e = t_6^f$ in Figure 7a). This lower I_{LC}/I_{SC} ratio translates into a relative cage occupancy ratio θ_{LC}/θ_{SC}~0.85, which indicates that LC is less populated with CH_4 molecules at t_6^f than at t_3^f. Intermediate spectra acquired at time t_a = 2 h and t_d = 75 h yield I_{LC}/I_{SC} ratios varying from ~2.8 to ~5.5. This suggests that the hydrate composition is heterogeneous with a relative cage population in CH_4 molecules varying heterogeneously with time. This is expected as the Raman probe cannot distinguish the secondary mixed hydrate formation from the initial hydrate phase still present. Further analysis using depth-profiling and/or Raman mapping would be useful to get a better insight on the heterogeneous distribution of the clathrate phases.

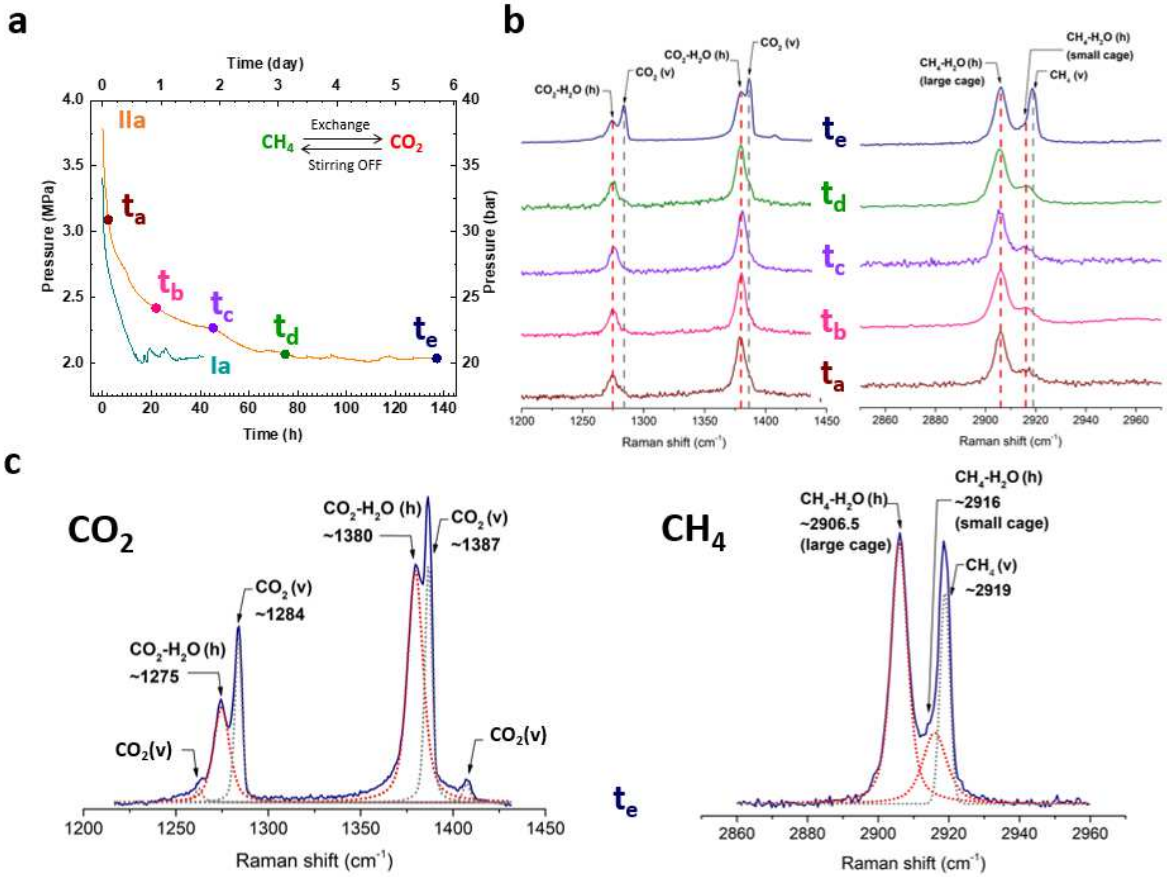

Figure 7: (a) Pressure evolution with time during CH_4-CO_2 exchange experiments (exp. Ia *vs* IIa) with 5 snapshots in time identified along the reaction (*ta-te*). (b) Corresponding Raman spectra depicting the time evolution of both the hydrate (h) and vapor (v) phases in CO_2 (1200-1450 cm^{-1}) and CH_4 (2860-2960 cm^{-1}) spectral regions during the exchange process and for the same position of the laser probe. (c) Enlargement of Raman spectra acquired at time *te* and subjected to the Raman band fitting procedure, allowing for clathrate structure and cage occupancy determination.

Raman spectroscopy is also utilized to monitor a portion of the downward total reactor pressure slope characteristic of the slow exchange process occurring in the isobaric experiment IVa (Figure 8). Raman

spectra are acquired every 3 days between days 6 and 19 (Figure 8a) and are subjected to the same fitting procedure as that shown for experiment IIa (Figure 7). The Raman signatures of CH_4-H_2O(h) and CO_2-H_2O(h) are detected together at day 6 while exhibiting weak intensities. The secondary hydrate CO_2-H_2O(h) keeps growing and is easily detected until day 19. The Raman signatures of CH_4 place the molecule within different environments as already described in section 3.1 (LC (~2906.5 cm^{-1}) and the SC (~2916.5 cm^{-1}) of clathrate sI, the gas phase (~2919 cm^{-1})), however with an additional seldom contribution of CH_4 dissolved in free water at ~2907.3 cm^{-1} (CH_4-H_2O(liq)). From the band intensity ratio of the peaks attributed to the LC and SC, one derives I_{LC}/I_{SC} ~ 2.5 at the end of step 3 of the CH_4-hydrate (i.e., at time t_3^f in exp. IVa, spectrum not shown here), thus the LC may be partially filled at the end of the parent hydrate formation. At day 6 of the exchange, we derive an integrated intensity ratio I_{LC}/I_{SC} ~ 0.9 (i.e., a cage occupancy ratio of θ_{LC}/θ_{SC} ~ 0.3), while an important peak due to CH_4 dissolved in water is observed. This suggests that the LCs are only partly occupied by CH_4 molecules (~30%). The remaining LCs may be occupied by CO_2 molecules that are known (in the pure CO_2-hydrate) to be preferentially trapped into the LC of structure sI [62]. Spectra collected between day 9 and day 19 show less contribution of dissolved methane. The integrated CH_4-H_2O(h) intensity ratio evolves from I_{LC}/I_{SC} ~ 1.7 to 1.1 (i.e. θ_{LC}/θ_{SC} ~ 0.6 to 0.4 and CH_4 in θ_{LC} ~ 56% to 38%) from day 9 to day 15 and further reduces to I_{LC}/I_{SC} ~ 0.2 at day 19. However, this latter value is affected by a high uncertainty due to the detection of a small quantity of CH_4 trapped in the clathrate phase. This Raman analysis suggests that the composition of the cage occupancy evolves slowly during the exchange by solid-state diffusion/secondary hydrate formation and that the continuous progression of a secondary hydrate phase is associated with the preferential incorporation of CO_2 into the LCs of structure sI. Dissociation of the primary CH_4 hydrate occurs during the first 50 h as evidenced by a 1.0 MPa pressure increase, which supports the subsequent formation of secondary mixed CO_2-CH_4 hydrates that will eventually allow for more CO_2 to be incorporated (i.e., hydrates with lower CH_4 ratio θ_{LC}/θ_{SC}). In contrast, experiment IIa shows no such pressure increase, which suggests that less CH_4 hydrates dissociate. Accordingly, the cage occupancy ratio derived from experiment IIa is higher (θ_{LC}/θ_{SC}~0.85) than that of experiment IVa (θ_{LC}/θ_{SC} ~ 0.4) at the end of the exchange. In addition to this, the initial parent CH_4-hydrate cage occupancy ratio is lower in IVa (I_{LC}/I_{SC} ~ 2.5 (IVa) *vs* I_{LC}/I_{SC} ~ 3.2 (IIa)) suggesting that less CH_4 molecules are present in the LC, and that more CO_2 can then be accommodated.

These results suggest different compositional partitioning within the hydrate phases, where a mixture of CO_2-rich secondary hydrates and remnant parent CH_4 hydrates makes up experiment IIa, whereas secondary mixed CO_2-CH_4 hydrates coexist with in remnant parent CH_4 hydrates in experiment IVa. Therefore, the Raman signal acquired in experiment IIa for CH_4 mainly reflects the composition of an unaltered parent hydrate and provides accordingly a higher θ_{LC}/θ_{SC} ratio.

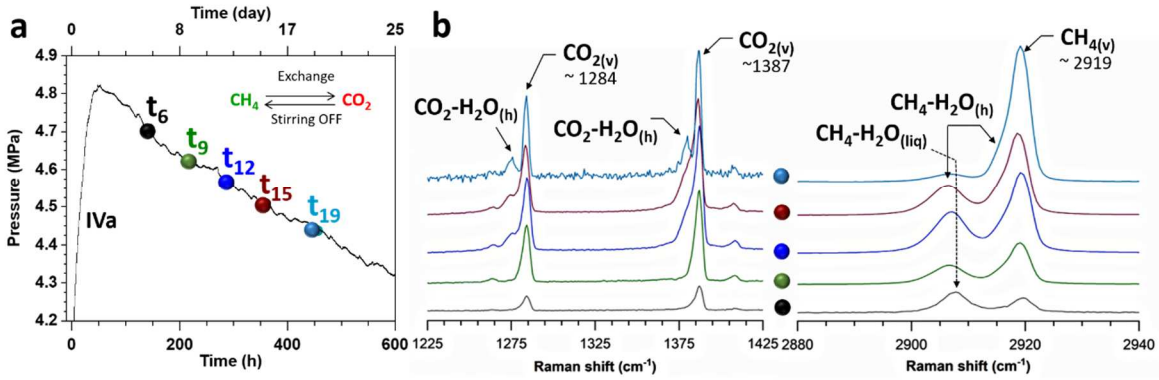

Figure 8: (a) Snapshots in time identified during the exchange process of experiment IVa and (b) corresponding Raman spectra showing the time evolution of both the hydrate (h) and vapor (v) phases in CO_2 (1200-1450 cm^{-1}) and CH_4 (2860-2960 cm^{-1}) spectral regions for days 6, 9, 12, 15, and 19.

In addition, the gas phase composition in experiment IVa can be inferred from CO_2(v) and CH_4(v) Raman band areas following the procedure described in Burke et al. (2001) [63] and using scattering cross sections of 1.5 and 7.5 for CO_2 (area of the two bands) and CH_4, respectively. Repeating the measurements and procedure several times, we derive an error of ± 2 mol% in CO_2 composition. The analysis of spectra acquired between days 6 and 15 of experiment IVa indicates a CO_2-rich gas phase with a composition slightly decreasing with time from y_{CO2}~ 59 to 58.4 mol%. When the same procedure is applied to experiment IIa, the concentration of CO_2(v) increases up to y_{CO2}~ 82 mol% at day 5. This result confirms that less CH_4(v) is released in the gas phase in experiment IIa.

3.5. Methane gas recovered with the gas mixture CO_2:N_2 20:80

Figure 9a displays the exchange kinetic curves of experiments IIIa and IIIb, describing the total reactor pressure decays followed upon (20%CO_2 + 80%N_2)(v) exposure (~12 MPa, 277 K) of a primary CH_4 hydrate (formed with Δp~5 MPa) within an unstirred or stirred environment, respectively. The pressure and temperature chosen for the exchange reaction (~12 MPa, 277 K) fall well within the stability field of the corresponding mixed hydrate [14] and that of the mixed (29%CH_4-57%N_2-14%CO_2) hydrate system, the equilibrium composition expected in our batch reactor (CSMGem calculation, Table 1). During the exchange with the binary mixture, the total reactor pressure decay curve follows a trend akin to that observed before for other unstirred experiments such as Ia and IIa, where the overall decay can be described as a two-segment curve (Figure 9a), described by a first steep fall (segment A-B) followed by a slower decline (segment C). The main difference resides in the steepness of the curve and in the fact that this first curve segment can further be broken down into two distinct portions as depicted in Figure 9b, which provides an enlargement of the first 18h of reaction for experiments IIIa and IIIb. Specifically, for experiment IIIa, the first curve segment (A) combines an initial pressure loss of ~1.2 MPa occurring during the first 12 minutes of reaction, followed by a small pressure burst of ~0.1 MPa over the next 10 min. The pressure loss corresponds to the rapid dissolution of CO_2(v) (and only marginally N_2(v)) in the free water available in the reactor (Table 1), which also may be enriched in dissolved CH_4 molecules. The subsequent change in fluid composition surrounding CH_4 hydrates modifies the chemical equilibrium and results in its destabilization, as evidenced by the small pressure burst of~0.1 MPa (during 10 min) occurring when CH_4 molecules are released in the gas phase. The second curve segment (B) is characterized by a smooth pressure decrease (loss of ~ 0.5 MPa over 17 h) likely due to the dissolution of gaseous species released during the previous chemical disequilibrium. This second segment curve (B) ends with a small pressure increase of ~0.1 MPa spanning over ~1h and indicating a new burst of CH_4 molecules released from the parent hydrate. Accordingly, total reactor pressure curve segments A and B follow similar pathways but over a longer time scale and in smaller magnitude for the latter because of the smaller chemical equilibrium disturbance and thus the smaller amounts of CH_4(v) released. Although the formation of secondary hydrates at the liquid parent-hydrate (or gas parent-hydrate) interface is not excluded, Raman spectra acquired at the end of the first curve segment (at t ~ 18 h only evidence the gas phase or dissolved signatures of CO_2, N_2, and CH_4 molecules. The third and last curve segment C exhibits the slowest pressure decline (~0.5 MPa in 680 h), during which diffusion-limited gas hydrate dissociation and re-formation processes occur. Raman spectra acquired at time t_{Raman} ~525 h (Figure 9c) confirm the coexistence of CO_2-H_2O(h) and CH_4-H_2O(h). However, the origin of CH_4-H_2O(h) (parent or secondary hydrate) cannot be deduced from the very weak signal recorded. In addition, the formation of N_2-H_2O(h) is not observed (Figure 9c). Note that the deterioration of the Raman signatures at the end of the reaction (~700 h) no longer allows the unambiguous identification of CH_4-H_2O(h).

In comparison, Schicks et al. [64] observed the formation of a secondary mixed CO_2-N_2 hydrate devoid of CH_4 in a similar batch experiment performed at 11.3 MPa, but monitored over a short timescale of ~48 h. In a distinct experiment conducted at 10.2 MPa, they showed the formation of a secondary hydrate containing CO_2, N_2, and CH_4 with a heterogeneous composition. They also noted in

a distinct additional experiment that no secondary hydrates could be detected below the exchange pressure of 9.8 MPa, i.e. below the end-pressure p_6^f of our experiment (~9.7 MPa). The effect of the unreacted melted ice particles at 278 K on the recovery and effective driving force to promote secondary hydrate formation was not investigated by the authors. Our results suggest that the exchange process upon exposure to CO_2-N_2 gas mixture leads principally to the dissolution of CO_2 and dissociation of the parent hydrate. However, as the initial amount of CO_2 is low (20% relative to N_2), and nitrogen remains principally in the gas phase, the unreacted free liquid water is not saturated with CO_2 gas to promote efficient clathrate formation. The parent hydrate starts to dissociate in order for the system to achieve equilibrium while the relative amount of unreacted water and parent CH_4-hydrate will control the effective driving force remaining after dissolution of the CO_2-N_2 gas mixture. Thus, the occurrence of free liquid water perturbs the straightforward interpretation of compositional information for the recovered fluid phase in terms of exchange rate.

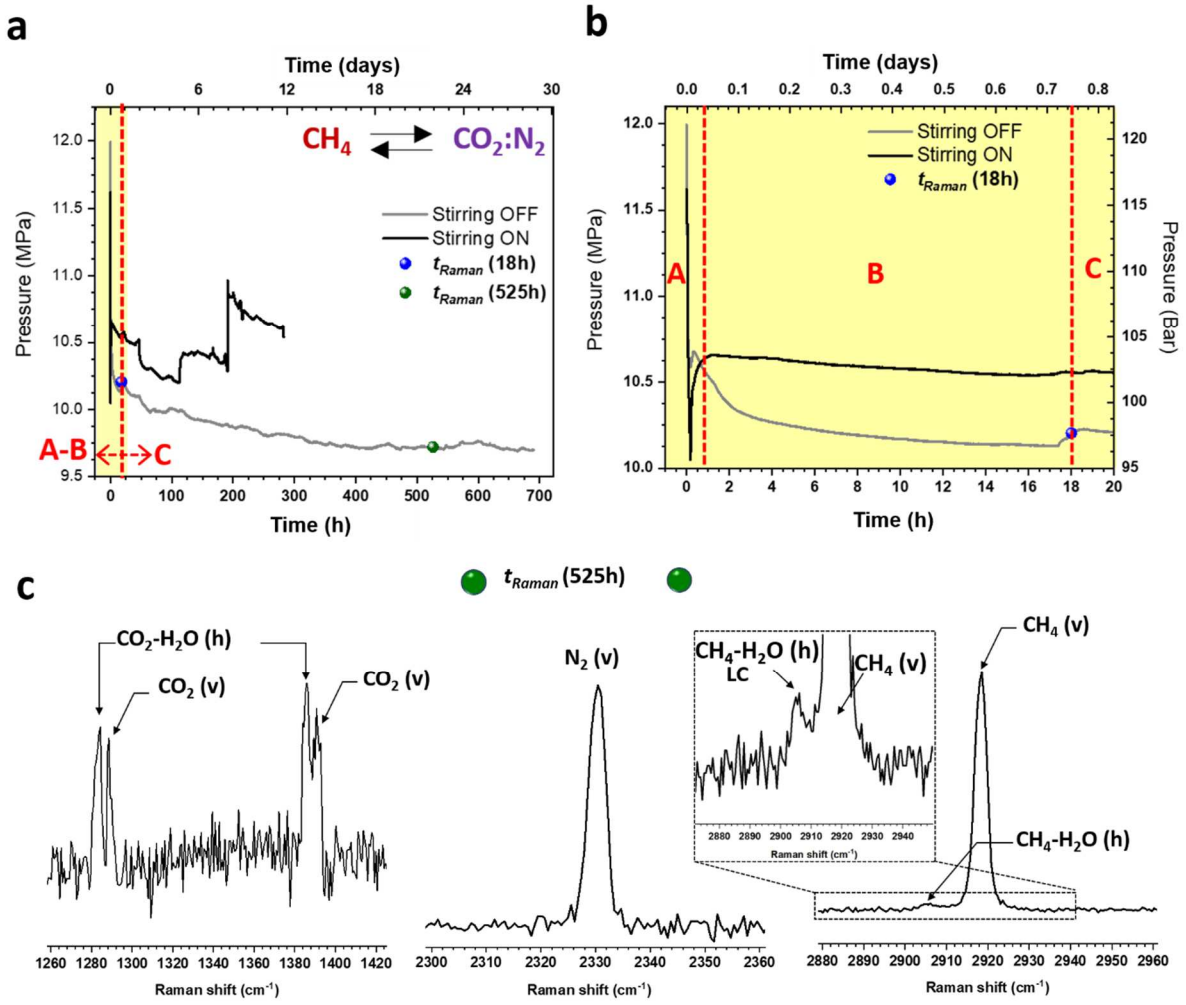

Figure 9: Pressure evolution during the exchange reaction between methane and 20%CO_2-80%N_2 gas mixture using different methods: under stirred conditions (Stirring ON) black line and without stirring (Stirring OFF) grey line. Enlarge view of the first ~15-20 h are displayed in (a) for the unstirred (left panel) and stirred (right panel) conditions. Complete kinetic curve is displayed in (a). The associated Raman spectra collected at time t_{Raman} ~ 525 h is indicated in (a) as a green dot. The Raman spectra are provided in panel (c) for the CO_2-clathrate (CO_2-H_2O (h)) with free CO_2 gas (CO_2 (v)), N_2 (v) for nitrogen in vapor phase and CH_4 (v) and CH_4-H_2O (h) for methane in the vapor and clathrate phases respectively.

Upon stirring (experiment IIIb), the exchange kinetic curve exhibits a distinct behavior than that of experiment IIIa (Figure 9b), which emerges only when comparing the two curve segments A. Specifically, the total reactor pressure curve of experiment IIIb exhibits a rapid pressure drop induced by CO_2 dissolution in free water, followed by a rapid (~1 h) and significant pressure increase (~0.6 MPa) that we attribute to the dissociation of an important fraction of the parent hydrate. This is in sharp contrast with the unstirred experiment (IIIa), where the parent hydrate only slightly decomposes within the first hour (~0.1 MPa), and then decreases smoothly over the next 40 h, which is consistent with system equilibration. Part C of the total reactor pressure curve of experiment IIIb is marked by a small pressure increase of 0.05 MPa during ~ 6 h, after which a smooth decrease of ~0.35 MPa during ~65 h occurs (Figure 9a). Thus, the first remaining parent hydrate dissociation step is followed by an equilibration step with dissolution of the species and reach of chemical equilibrium in the solution. The remaining 170 h feature two dissociation events (+0.2 MPa in 8 h / +0.5 MPa in 1.5 min) separated by ~70 h, each followed by downward pressure slopes, the latter being more pronounced (~0.3 MPa in 85 h) than the former. These variations in pressure originate from the activation of the stirrer in experiment IIIb, which accentuate the stochastic nature of the process. Although experiment IIIb is conducted in the same conditions as experiment IIIa, the system does not reach equilibrium (Table 1 last column). Stirring is thus efficient during the first part of the reaction, promoting the rapid dissolution of the species and dissociation of the main part of the parent hydrate, but its efficiency reduces with time and as it only helps dissociating the remaining hydrate or initiating the formation of a new hydrate at longer times.

4. Conclusion

In this work, kinetic experiments of gas exchange in CH_4-hydrate formed from liquid water were conducted in a new high-pressure optical reactor chamber equipped with mechanical stirring and cooling/heating capabilities. Four distinct mechanisms explain the kinetic curves describing exchange reactions: a decoupled gas exchange where 1) CH_4 hydrate dissociates and 2) CO_2 is rapidly dissolved into the remaining free liquid water, 3) secondary CO_2-rich hydrates form either from liquid water-CO_2(v) interaction or from dissolved CO_2, and 4) a solid-state exchange reaction occurs within the hydrates, where a molecule of CO_2 replaces a molecule of CH_4 by shrinking core solid state diffusion [31]. We evidence that low driving forces (Δp) applied to form CH_4-hydrates improved the exchange kinetic by a factor of ~3, for which there is a higher relative amount of free H_2O(liq) (277 K); the kinetic is further improved in all cases investigated with CO_2 injection when stirring is applied. The mechanism 1), 2) and 3) are thus privileged. When only methane hydrate is present at the onset of the exchange (isobaric formation), a rapid dissociation associated with a sudden pressure increase brings the system above the equilibrium line of CH_4 hydrate. Then mechanisms 2), 3), and 4) are privileged with the rapid absorption of CO_2 followed by the slow exchange by CO_2-CH_4 solid state diffusion or by secondary CO_2-rich hydrate formation. The net result is a slower exchange kinetic (2 orders of magnitude) compared to the situation where the amount of the parent methane hydrate is small and initially coexists with liquid water. Therefore, it appears that the exchange reaction kinetic is driven by the initial relative partitioning CH_4(h)/H_2O(liq)/CO_2(v), that is equivalent to a relative CH_4 enrichment of the vapor phase after the rapid partial dissociation of the parent CH_4-hydrate. Furthermore, Raman analyses point toward a heterogeneous composition (CO_2-CH_4) evolving with time for secondary hydrates, with CO_2 being preferentially incorporated into the large cavity of the structure sI.

The exposure of CH_4-hydrate to a binary CO_2-N_2 gas mixture proves to be less efficient with a lower kinetic constant (one order of magnitude lower) than with CO_2. The relative amounts of unreacted water and parent CH_4-hydrate control the effective driving force remaining after dissolution of the CO_2-N_2 gas mixture for the formation of secondary CO_2-rich hydrate or CO_2-CH_4 exchange by solid state diffusion. The Raman analysis proves the coexistence of CO_2 and CH_4 clathrates during the reaction, although the deterioration of the Raman signatures at the end of the reaction (~700 h) could no longer allow the unambiguous identification of CH_4 clathrates.

These results may help optimizing recovery processes in field trial experiments, where conditions of depressurization and exchange reactions still need to be improved. Laboratory studies involving conditions close to natural systems, where both hydrates and liquid water coexist, are needed to improve exchange processes, limit the risk of geo-hazards with unstable secondary hydrates, and better assess the parameters influencing the overall energy efficiency and energy cost of CH_4 recovery processes in gas hydrate field trials..

Supplementary Materials: Supplementary data to this article can be found online at XXX

Author Contributions: Conceptualization, Q-DL, BC; methodology, Q-DL, BC, CP; data treatment, all authors; writing—original draft preparation, Q-DL, LL, BC; writing—review and editing, all authors; project administration and funding acquisition, BC. All authors have read and agreed to the published version of the manuscript.

Funding: This research was partly supported by the Université de Lille and the Région Hauts-de-France with a PhD grant n°17006757.

Acknowledgments: the authors acknowledge the Région Hauts-de-France, the Ministère de l'Enseignement Supérieur et de la Recherche and the European Fund for Regional Economic Development for their financial support (CPER CLIMIBIO). The authors also acknowledge funding from the Interreg 2 Seas program 2014-2020 co-funded by the European Regional Development Fund under subsidy contract Carbon2Value 2S01-094 (2017-2021).

Conflicts of Interest: The authors declare no conflict of interest.

References

1. M. Bui, C. S. Adjiman, A. Bardow, E. J. Anthony, A. Boston, S. Brown, et al., "Carbon capture and storage (CCS): The way forward," *Energy and Environmental Science* **2018**, *vol. 11*, pp. 1062–1176. doi: https://doi.org/10.1039/C7EE02342A
2. M. K. Mondal, H. K. Balsora, and P. Varshney, "Progress and trends in CO_2 capture/separation technologies: A review," *Energy* **2012**, *vol. 46*, pp. 431–441. doi: https://doi.org/10.1016/j.energy.2012.08.006
3. D.-Y. Koh, H. Kang, J.-W. Lee, Y. Park, Se-J. Kim, J. Lee, et al., "Energy-efficient natural gas hydrate production using gas exchange," *Applied Energy* **2016**, *vol. 162*. pp. 114–130. doi https://doi.org/10.1016/j.apenergy.2015.10.082
4. CB. Bavoh, B. Lal, H. Osei, KM. Sabil, H. Mukhtar "A review on the role of amino acids in gas hydrate inhibition, CO2 capture and sequestration, and natural gas storage" *J Nat Gas Sci Eng* **2019**; *vol. 64*, pp. 52–71. https://doi.org/10.1016/j.jngse.2019.01.020.
5. Kumar R, Roy S, Bhattacharjee G, Choudhary N, Kumar A, Kumar R, et al. "A Process for dissociation of hydrates in presence of additives or hydrate dissociation promoters". *US 2019 / 0031943 A1, 2019*
6. R. Boswell, D. Schoderbek, T. S. Collett, S. Ohtsuki, M. White, and B. J. Anderson, "The Iġnik Sikumi field experiment, Alaska North Slope: Design, operations, and implications for CO_2-CH_4 exchange in gas hydrate reservoirs," *Energy and Fuels* **2017**, *vol. 31*, pp. 140–153. Doi: https://doi.org/10.1021/acs.energyfuels.6b01909
7. R. Boswell, K. Yamamoto, S. R. Lee, T. Collett, P. Kumar, and S. Dallimore, "Methane Hydrates," in *Future Energy: Improved, Sustainable and Clean Options for our Planet*, 2013, pp. 159–178. doi: https://doi.org/10.1016/B978-0-08-099424-6.00008-9
8. R. Boswell, J. Yoneda, and W. F. Waite, "India National Gas Hydrate Program Expedition 02 summary of scientific results: Evaluation of natural gas-hydrate-bearing pressure cores," *Mar. Pet. Geol.* **2019**, *vol. 108*, pp. 143–153. Doi: https://doi.org/10.1016/j.marpetgeo.2018.10.020

9. P. L. Stanwix, N. M. Rathnayake, F. P. P. De Obanos, M. L. Johns, Z. M. Aman, and E. F. May, "Characterising thermally controlled CH_4-CO_2 hydrate exchange in unconsolidated sediments," *Energy Environ. Sci.* **2018**, *vol. 11*, pp. 1828–1840. Doi: https://doi.org/10.1039/C8EE00139A
10. E. D. Sloan Jr. and C. A. Koh, *Clathrate Hydrates of Natural Gases*. CRC Press, Boca Raton, FL, USA, **2007**.
11. W. F. Kuhs, B. Chazallon, P. G. Radaelli, and F. Pauer, "Cage occupancy and compressibility of deuterated N2-clathrate hydrate by neutron diffraction," *J. Incl. Phenom. Mol. Recognit. Chem.* **1997**, *vol. 29*, pp. 65–77. Doi: https://doi.org/10.1023/A:1007960217691
12. B. Chazallon and W. F. Kuhs, "In situ structural properties of N2-, O2-, and air-clathrates by neutron diffraction," *J. Chem. Phys.* **2002**, *vol. 117*, pp. 308–320. Doi: https://doi.org/10.1063/1.1480861
13. R. Anderson, M. Llamedo, B. Tohidi, and R. W. Burgass, "Experimental measurement of methane and carbon dioxide clathrate hydrate equilibria in mesoporous silica," *J. Phys. Chem. B*. **2003**, *vol. 107*, pp. 3507–3514. Doi: https://doi.org/10.1021/jp0263370
14. B. Chazallon and C. Pirim, "Selectivity and CO_2 capture efficiency in CO_2-N_2 clathrate hydrates investigated by in-situ Raman spectroscopy," *Chem. Eng. J.* **2018**, *vol. 342*, pp. 171–183. Doi: https://doi.org/10.1016/j.cej.2018.01.116
15. K. Ohgaki, K. Takano, H. Sangawa, T. Matsubara, and S. Nakano, "Methane exploitation by carbon dioxide from gas hydrates. Phase equilibria for CO_2-CH_4 mixed hydrate system.," *J. Chem. Eng. JAPAN*. **1996**, vol. 29, pp. 478–483. Doi: https://doi.org/10.1252/jcej.29.478
16. S. Hirohama, Y. Shimoyama, A. Wakabayashi, S. Tatsuta, N. Nishida, "Conversion of CH_4-Hydrate to CO_2-Hydrate in Liquid CO_2," *J. Chem. Eng. Japan*, **1996**, *vol 29*, pp. 1014-1020. Doi: https://doi.org/10.1252/jcej.29.1014
17. H. Komatsu, M. Ota, R. L. Smith, and H. Inomata, "Review of CO_2-CH_4 clathrate hydrate replacement reaction laboratory studies - Properties and kinetics," *J. Taiwan Inst. Chem. Eng.* **2013**, *vol. 44*, pp. 517–537. Doi: https://doi.org/10.1016/j.jtice.2013.03.010
18. Park, Y.; Kim, D.; Lee, J.; Huh, D.; Park, K.; Lee, J. et al., "Sequestering carbon dioxide into complex structures of naturally occurring gas hydrates. *Proc. Natl. Acad. Sci. USA* 2006, *103*, 12690–12694. Doi: https://doi.org/10.1073/pnas.0602251103
19. H. Lee, Y. Seo, Y. T. Seo, I. L. Moudrakovski, and J. A. Ripmeester, "Recovering Methane from Solid Methane Hydrate with Carbon Dioxide," *Angew. Chemie - Int. Ed.* **2003**, *vol. 42*, pp. 5048–5051. Doi: https://doi.org/10.1002/anie.200351489
20. J. H. Yoon, T. Kawamura, Y. Yamamoto, and T. Komai, "Transformation of methane hydrate to carbon dioxide hydrate: In situ Raman spectroscopic observations," *J. Phys. Chem. A* **2004**, *vol. 108*, pp. 5057–5059. Doi: https://doi.org/10.1021/jp049683l
21. M. Ota, Y. Abe, M. Watanabe, R. L. Smith, and H. Inomata, "Methane recovery from methane hydrate using pressurized CO_2," *Fluid Phase Equilib.* **2005**, *vol. 228–229*, pp. 553–559. Doi: https://doi.org/10.1016/j.fluid.2004.10.002
22. M. Ota, K. Morohashi, Y. Abe, M. Watanabe, R. L. Smith, Jr., and H. Inomata, "Replacement of CH_4 in the hydrate by use of liquid CO_2," *Energy Convers. Manag.* **2005**, *vol. 46*, pp. 1680–1691. Doi: https://doi.org/10.1016/j.enconman.2004.10.002
23. M. Ota, Takeomi Saito, Tsutomu Aida, Masaru Watanabe, Yoshiyuki Sato, Richard L, Smith Jr., et al., "Macro and microscopic CH_4–CO_2 replacement in CH_4 hydrate under pressurized CO_2," *AIChE J.* **2007**, *vol. 53*, pp. 2715–2721. Doi: https://doi.org/10.1002/aic.11294
24. X. Zhou, S. Fan, D. Liang, and J. Du, "Determination of appropriate condition on replacing methane from hydrate with carbon dioxide," *Energy Convers. Manag.* **2008**, *vol. 49*, pp. 2124–2129. Doi: https://doi.org/10.1016/j.enconman.2008.02.006
25. B. R. Lee, C. A. Koh, and A. K. Sum, "Quantitative measurement and mechanisms for CH_4 production from hydrates with the injection of liquid CO_2," in *Physical Chemistry Chemical Physics*, **2014**, *vol. 16*, pp. 14922–14927. Doi: https://doi.org/10.1039/C4CP01780C
26. X. Wang, A. J. Schultz, and Y. Halpern, "Kinetics of methane hydrate formation from polycrystalline deuterated ice," *J. Phys. Chem. A* **2002**, *vol. 106*, pp. 7304–7309. Doi: https://doi.org/10.1021/jp025550t

27. J. M. Schicks, M. Luzi, and B. Beeskow-Strauch, "The conversion process of hydrocarbon hydrates into CO_2 hydrates and vice versa: Thermodynamic considerations," *J. Phys. Chem. A* **2011**, *vol. 115*, pp. 13324–13331. Doi: https://doi.org/10.1021/jp109812v
28. D. Bai, X. Zhang, G. Chen, and W. Wang, "Replacement mechanism of methane hydrate with carbon dioxide from microsecond molecular dynamics simulations," *Energy Environ. Sci.* **2012**, *vol. 5*, pp. 7033–7041. Doi: https://doi.org/10.1039/C2EE21189K
29. Y. Iwai, H. Nakamura, and M. Hirata, "Molecular dynamics simulation of replacement of methane hydrate with carbon dioxide," *Mol. Simul.* **2012**, *vol. 38*, pp. 481–490. Doi: https://doi.org/10.1080/08927022.2011.647817
30. A. Falenty, J. Qin, A. N. Salamatin, L. Yang, and W. F. Kuhs, "Fluid composition and kinetics of the in situ replacement in CH_4-CO_2 hydrate system," *J. Phys. Chem. C* **2016**, *vol. 120*, pp. 27159–27172. Doi: https://doi.org/10.1021/acs.jpcc.6b09460
31. A. N. Salamatin, A. Falenty, and W. F. Kuhs, "Diffusion Model for Gas Replacement in an Isostructural CH_4-CO_2 Hydrate System," *J. Phys. Chem. C.* **2017**, *vol. 121*, pp. 17603–17616. Doi: https://doi.org/10.1021/acs.jpcc.7b04391
32. C. G. Xu, J. Cai, Y. S. Yu, K. F. Yan, and X. Sen Li, "Effect of pressure on methane recovery from natural gas hydrates by methane-carbon dioxide replacement," *Appl. Energy* **2018**, *vol. 217*, pp. 527–536. Doi: https://doi.org/10.1016/j.apenergy.2018.02.109
33. M. Cha, K. Shin, H. Lee, I. L. Moudrakovski, J. A. Ripmeester, and Y. Seo, "Kinetics of methane hydrate replacement with carbon dioxide and nitrogen gas mixture using in situ NMR spectroscopy," *Environ. Sci. Technol.* 2015, *vol. 49*, pp. 1964–1971. Doi: https://doi.org/10.1021/es504888n
34. Youngjune Park, Do-Youn Kim, Jong-Won Lee, Dae-Gee Huh, Keun-Pil Park, Jaehyoung Lee et al., "Sequestering carbon dioxide into complex structures of naturally occurring gas hydrates," *Proc. Natl. Acad. Sci. U. S. A.* **2006**, *vol. 103*, pp. 12690–12694. Doi: https://doi.org/10.1073/pnas.0602251103
35. G. Ersland, J. Husebø, A. Graue, B. A. Baldwin, J. Howard, and J. Stevens, "Measuring gas hydrate formation and exchange with CO_2 in Bentheim sandstone using MRI tomography," *Chem. Eng. J.* **2010**, *vol. 158*, pp. 25–31. Doi: https://doi.org/10.1016/j.cej.2008.12.028
36. S. Lee, Y. Lee, J. Lee, H. Lee, and Y. Seo, "Experimental verification of methane-carbon dioxide replacement in natural gas hydrates using a differential scanning calorimeter," *Environ. Sci. Technol.* **2013**, *vol. 47*, pp. 13184–13190. Doi: https://doi.org/10.1021/es403542z
37. Y. T. Tung, L. J. Chen, Y. P. Chen, and S. T. Lin, "In situ methane recovery and carbon dioxide sequestration in methane hydrates: A molecular dynamics simulation study," *J. Phys. Chem. B*, **2011**, *vol. 115*, pp. 15295–15302. Doi: https://doi.org/10.1021/jp2088675
38. A. Hassanpouryouzband, J. Yang, B. Tohidi, E. Chuvilin, V. Istomin, B. A. Bukhanov, et al. "CO_2 Capture by Injection of Flue Gas or CO_2-N_2 Mixtures into Hydrate Reservoirs: Dependence of CO_2 Capture Efficiency on Gas Hydrate Reservoir Conditions," *Environ. Sci. Technol.* **2018**, *vol. 52*, pp. 4324–4330. Doi: https://doi.org/10.1021/acs.est.7b05784
39. A. Hassanpouryouzband, J. Y., B. Tohidi, E. Chuvilin, V. Istomin, B. A. Bukhanov, and A. Cheremisin, "Insights into CO_2 Capture by Flue Gas Hydrate Formation: Gas Composition Evolution in Systems Containing Gas Hydrates and Gas Mixtures at Stable Pressures," *ACS Sustain. Chem. Eng.* **2018**, *vol. 6*, pp. 5732–5736. Doi: https://doi.org/10.1021/acssuschemeng.8b00409
40. S. H. B. Yang, P. Babu, S. F. S. Chua, and P. Linga, "Carbon dioxide hydrate kinetics in porous media with and without salts," *Appl. Energy* **2016**, *vol. 162*, pp. 1131–1140. Doi: https://doi.org/10.1016/j.apenergy.2014.11.052
41. Q. Yuan, C. -Yu Sun, X. Yang, P.C. Ma, Z.-W. Ma, B. Liu, Q.-L. Ma, L. –Y. Yang, G.J. Chen, "Recovery of methane from hydrate reservoir with gaseous carbon dioxide using a three-dimensional middle-size reactor," *Energy* **2012**, *vol. 40*, pp. 47–58. Doi: https://doi.org/10.1016/j.energy.2012.02.043
42. Q. Yuan, C.Y. Sun, B. Liu, X. Wang, Z.W. Ma, Q.L. Ma, L.Y. Yang, G.J. Chen, Q.P. Li, S. Li, K. Zhang, "Methane recovery from natural gas hydrate in porous sediment using pressurized liquid

CO_2," *Energy Convers. Manag.* **2013**, *vol. 67*, pp. 257–264. Doi: https://doi.org/10.1016/j.enconman.2012.11.018

43. Y. Chen, Y. Gao, Y. Zhao, L. Chen, C. Dong, and B. Sun, "Experimental investigation of different factors influencing the replacement efficiency of CO_2 for methane hydrate," *Appl. Energy*, Oct. **2018**, *vol. 228*, pp. 309–316. Doi: https://doi.org/10.1016/j.apenergy.2018.05.126
44. J. Yang, A. Okwananke, B. Tohidi, E. Chuvilin, K. Maerle, V. Istomin, B. Bukhanov, A. Cheremisin, "Flue gas injection into gas hydrate reservoirs for methane recovery and carbon dioxide sequestration," *Energy Conversion and Management.* **2017**, *vol. 136*, pp. 431–438. Doi: https://doi.org/10.1016/j.enconman.2017.01.043
45. A. Okwananke, A. Hassanpouryouzband, M. V. Farahania, J. Yang, B. Tohidi, E. Chuvilin, V. Istomin, B. Bukhanov, "Methane recovery from gas hydrate-bearing sediments: An experimental study on the gas permeation characteristics under varying pressure," *J. Pet. Sci. Eng.* **2019**, *vol. 180*, pp. 435–444. Doi: https://doi.org/10.1016/j.petrol.2019.05.060
46. C. Deusner, N. Bigalke, E. Kossel, and M. Haeckel, "Methane Production from Gas Hydrate Deposits through Injection of Supercritical CO2," *Energies.* **2012**, *vol. 5*, pp. 2112–2140. Doi: https://doi.org/10.3390/en5072112
47. S. Adisasmito, R. J. Frank, and E. D. Sloan, "Hydrates of Carbon Dioxide and Methane Mixtures," *J. Chem. Eng. Data*. **1991**, *vol. 36*, pp. 68–71. Doi: https://doi.org/10.1021/je00001a020
48. A. Van Cleeff and G. A. M. Diepen, "Gas hydrates of Nitrogen and Oxygen" *Recueil des Travaux Chimiques des Pays-Bas*. **1960**, *vol. 79*, pp. 582-586. doi: https://doi.org/10.1002/recl.19600790606
49. Y. Lee, S. Lee, J. Lee, and Y. Seo, "Structure identification and dissociation enthalpy measurements of the CO2+N2 hydrates for their application to CO_2 capture and storage," *Chem. Eng. J.* **2014**, *vol. 246*, pp. 20–26. Doi: https://doi.org/10.1016/j.cej.2014.02.045
50. K. Yasuda and R. Ohmura, "Phase Equilibrium for Clathrate Hydrates Formed with Methane, Ethane, Propane, or Carbon Dioxide at Temperatures below the Freezing Point of Water," *J. Chem. Eng. Data*. **2008**, *vol. 53*, pp. 2182–2188. Doi: https://doi.org/10.1021/je800396v
51. B. Chazallon, C. Focsa, J. L. Charlou, C. Bourry, and J. P. Donval, "A comparative Raman spectroscopic study of natural gas hydrates collected at different geological sites," *Chem. Geol.* **2007**, *vol. 244*, pp. 175–185. Doi: https://doi.org/10.1016/j.chemgeo.2007.06.012
52. A. K. Sum, R. C. Burruss, and E. D. Sloan, "Measurement of Clathrate Hydrates via Raman Spectroscopy," *J. Phys. Chem. B* 1997, *vol. 101*, pp. 7371–7377. Doi: https://doi.org/10.1021/jp970768e
53. J. Qin and W. F. Kuhs, "Quantitative analysis of gas hydrates using Raman spectroscopy," *AIChE J.* **2013**, *vol. 59*, pp. 2155–2167. Doi: https://doi.org/10.1002/aic.13994
54. L. N. Legoix, L. Ruffine, C. Deusner, and M. Haeckel, "Experimental study of mixed gas hydrates from gas feed containing CH_4 , CO_2 and N_2: Phase equilibrium in the presence of excess water and gas exchange," *Energies*, 2018, *vol. 11*. doi: https://doi.org/10.3390/en11081984
55. Y. Arai, G.-I. Kaminishi, and S. Saito, "The experimental determination of the P-V-T-X relations for the Carbon dioxide-Nitrogen and the Carbon dioxide-Methane systems" *J. Chem. Eng. Japan* **1971**, *vol. 4*, pp. 113–122. Doi: https://doi.org/10.1252/jcej.4.113
56. L. A. Stern, S. Circone, S. H. Kirby, and W. B. Durham, "Anomalous preservation of pure methane hydrate at 1 atm," *J. Phys. Chem. B* **2001**, *vol. 105*, pp. 1756–1762. Doi: https://doi.org/10.1021/jp003061s
57. S. O. Yang, I. M. Yang, Y. S. Kim, and C. S. Lee, "Measurement and prediction of phase equilibria for water+CO_2 in hydrate forming conditions," *Fluid Phase Equilib.* **2000**, *vol. 175*, pp. 75–89. Doi: https://doi.org/10.1016/S0378-3812(00)00467-2
58. P. Servio and P. Englezos, "Effect of temperature and pressure on the solubility of carbon dioxide in water in the presence of gas hydrate," *Fluid Phase Equilib.* **2001**, *vol. 190*, pp. 127–134. Doi: https://doi.org/10.1016/S0378-3812(01)00598-2
59. R. Ohmura, S. Matsuda, T. Uchida, T. Ebinuma, and H. Narita, "Clathrate hydrate crystal growth in liquid water saturated with a guest substance: Observations in a methane + water system," *Cryst. Growth Des.* **2005**, *vol. 5*, pp. 953–957. Doi: https://doi.org/10.1021/cg049675u

60. B. Kvamme, "Thermodynamic Limitations of the CO_2/N_2 Mixture Injected into CH_4 Hydrate in the Ignik Sikumi Field Trial," *J. Chem. Eng. Data* **2016**, *vol. 61*, pp. 1280–1295. Doi: https://doi.org/10.1021/acs.jced.5b00930
61. G. Herzberg, "Infrared and Raman spectra of polyatomic molecules," *Molecular spectra and molecular structure* 1945, *vol: 2*.
62. W. F. Kuhs, B. Chazallon, A. Klapproth, and F. Pauer, "Filling-Isotherms in Clathrate-Hydrates.," *Rev. HIGH Press. Sci. Technol.* **1998**, *vol. 7*, pp. 1147–1149. Doi: https://doi.org/10.4131/jshpreview.7.1147
63. E. A. J. Burke, "Raman microspectrometry of fluid inclusions," *Lithos*. **2001**, vol. 55, pp. 139–158. doi: https://doi.org/10.1016/S0024-4937(00)00043-8
64. J. M. Schicks, B. Strauch, K. U. Heeschen, E. Spangenberg, and M. Luzi-Helbing, "From Microscale (400 μl) to Macroscale (425 L): Experimental Investigations of the CO 2 /N 2 -CH 4 Exchange in Gas Hydrates Simulating the Iġnik Sikumi Field Trial," *J. Geophys. Res. Solid Earth*, **2018**, *vol. 123*, pp. 3608–3620. Doi: https://doi.org/10.1029/2017JB015315

SUPPLEMENTARY MATERIAL

Influence of the initial CH_4-hydrate system properties on CO_2 capture kinetics

Quang-Du Le [1], Carla T. Rodriguez [1], Ludovic Nicolas Legoix [1], Claire Pirim [1] and Bertrand Chazallon [1,*]

[1] Université de Lille, CNRS, UMR 8523 – PhLAM – Laboratoire de Physique des Lasers, Atomes et Molécules, CERLA – Centre d'Etudes et de Recherche Lasers et Applications, F-59000, Lille, France; quang-du.le@univ-lille.fr (Q.D.L); carla-thais.rodriguez-machine@univ-lille.fr (C.T.R); ludovic.legoix@univ-lille.fr (L.N.L.) ; claire.pirim@univ-lille.fr (C.P)

* Correspondence to bertrand.chazallon@univ-lille.fr; Tel.: +33 (0) 3 20 33 64 68 (B.C.)

Appendix A: Mass balance calculation

At any given moment, the initial quantity of gas molecules is distributed between all three phases: gas (G), liquid (L), and solid hydrate (H). Thus, in equilibrium, the quantity of gas in the hydrate phase can be determined from a mass balance calculation according to the following equation:

$$n_{i,0}^{initial} = n_i^G + n_i^L + n_i^H \quad (1)$$

where $n_{i,0}^{initial}$ is the initial mole number of gas (i) injected into the reactor, and n_i^G, n_i^L, n_i^H are the mole numbers of gas (i: CO_2, CH_4) contained in each of the three phases, respectively.

The amount gas dissolved into the liquid phase (water) is estimated from its corresponding gas solubility data, whereas the mole number of gas in the gas phase is calculated using an equation of state approach as outlined in the next sections.

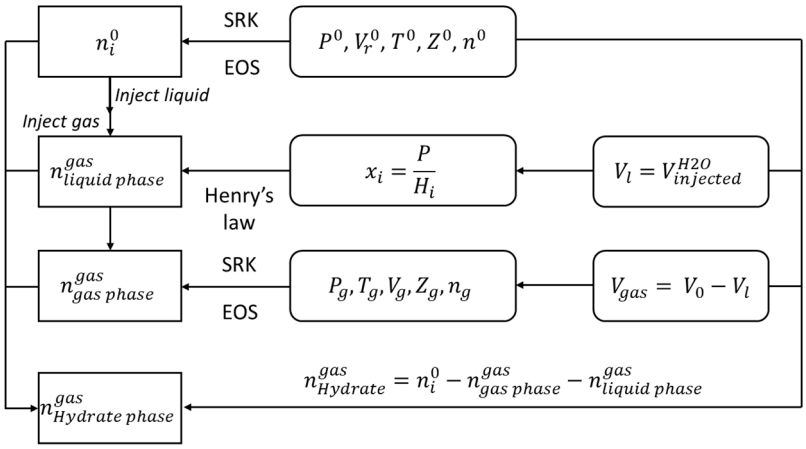

Figure 1: Flow chart describing mass balance calculations

a). Calculation of compressibility factor

The compressibility factor in the gas phase at a given equilibrium state can be calculated from Eq. (2) combined with a suitable equation of state (EOS), e.g., a classical cubic EOS. For this study, the Soave-Redlich and Kwong (SRK) EOS has been used with parameters sourced from Danesh [65], given in Table 1.

$$Z(T,P,x) = \frac{PV}{nRT} \tag{2}$$

with $n \equiv n^G$ (at each time step) and T, P, V are the temperature, pressure and phase volume, $x = (x_{CO2}, x_{N2}, x_{CH4})$, represents the gas components of the mixture with x_i the mol fraction of component i, n the total mole number in the gas mixture, and R the universal gas constant.

Table 1: SRK parameters [65] (Tc, Pc, ω, k) stands for critical temperature, critical pressure, intermolecular interaction potential, mixing parameter, respectively

j	Tc(K)	Pc(bar)	ω	k(N_2/j)	k(CO_2/j)	k(CH_4/j)
N_2	126.20	34.00	0.03772	0	-0.03	0.03
CO_2	304.21	73.83	0.22362	-0.03	0	0,0933
CH_4	190.56	45.99	0.01155	0.03	0,0933	0

b). Calculation of the solubility of gases in liquid phase

For treating gas solubility in our system, the unsymmetrical approach is used and combined with the unsymmetrical convention (Henry's law approach), which corresponds to an infinite dilution

reference (i.e. the activity coefficients of the gas molecules into the water equal to unity). The equilibrium condition reads:

$$P = x_i H_i \tag{3}$$

where H_i is Henry's law constant. It is expressed by means of the following relation:

$$H_i = H_{i,Psat} exp\left(\frac{v_i^{\infty}(P - P_i^{sat})}{RT}\right) \tag{4}$$

The so-called solubility models enable the calculation of Henry's law constant. The Henry's law constant is determined at the saturated vapor pressure of the pure solvent ($H_{i,Psat}$). Thus, the Poynting factor corrects for the pressure difference between P_{sat} of the pure solvent (water) and the system pressure P. The partial molar volume of gas *i* at infinite dilution (v_i^{∞}) can be calculated from a correlation proposed by Vidal et al. [66,67]. However, it is fixed here to 32 $cm^3.mol^{-1}$ for the majority of the components.

Holder et al. and Holder and Grigoriou [68,69] proposed the following correlation for Henry's constant at saturation with temperature:

$$H_{i,Psat} = exp\left(A + \frac{B}{T}\right) \tag{4}$$

The coefficients A and B are compiled in Table 2. The temperature is expressed in Kelvins and Henry's constant is given in atmospheres.

Table 2: Constants for calculating Henry's constant by Holder et al. [69]

Gas	A	B	V_i^{∞} (Cm^3/mole)
CH_4	15.826277	-1559.0631	32
CO_2	14.283146	-2050.3269	32
N_2	17.934347	-1933.381	32

Appendix B: Raman spectral parameters obtained after deconvolution and baseline treatment of raw Raman spectra for CO_2, CH_4 and N_2

Band's assignment	(ν^-) CO_2-hydrate	(ν^-) CO2 gas	(ν^+) CO_2-hydrate	(ν^+) CO2 gas	(ν_1) LC CH_4-hydrate	(ν_1) SC CH4-hydrate	(ν_1) gas (CH4)	(ν_1) dissolved CH4 in water	N_2 gas
Position (cm^{-1})	1275	1284	1380	1387	2906.5	2916.5	2919	2907.3	2330

Band width (cm^{-1})	9	4.5	9	4.5	6.5	5.5	3.5	5	4

References

65. A. Danesh, *PVT and phase behaviour of petroleum reservoir fluids*. Elsevier, 1998.
66. Vidal, J., Allieu, Y., Fassio, B., Adrey, J., Goalard, C., Réduction du spondylolisthésis par le matériel de Harrington. Proceedings of the SICOT. **1973**, pp. 646–647.
67. Vidal, J., Goalard, C., Escare, P., Allieu, Y., Normalisation d'une prothèse de toute l'extrémité supérieure du fémur. J Chir. **1973**, vol. 106, pp. 125–134.
68. G. D. Holder, G. Corbin, and K. D. Papadopoulos, "Thermodynamic and Molecular Properties of Gas Hydrates from Mixtures Containing Methane, Argon, and Krypton," *Ind. Eng. Chem. Fundam.* **1980**, vol. 19, pp. 282–286. Doi: https://doi.org/10.1021/i160075a008
69. G. D. Holder and G. C. Grigoriou, "Hydrate dissociation pressures of (methane + ethane + water) existence of a locus of minimum pressures," *J. Chem. Thermodyn.* 1980, vol. 12, pp. 1093–1104. Doi: https://doi.org/10.1016/0021-9614(80)90166-4